A final report submitted in partial fulfillment of the requirements for the Marshall Plan Scholarship

Development of an Implantable Biosensor for Rejection Detection and Long-term Monitoring in Cardiac Transplants

submitted by

Tibor Wladimir BSc.

Supervisor:

Georg Wieselthaler, MD, Peter Ertl, PhD, Erik Reimhult, PhD

DEPARTMENT OF SURGERY

UNIVERSITY OF CALIFORNIA, SAN FRANCISCO

Acknowledgements

First, I would like to thank to the generous financial support of the Austrian Marshall Plan Foundation. This work would not be as it is now without the great support I have received during the last months. Therefore I would like to express my special appreciation to following people and institutions:

- Erik Reimhult for giving me the opportunity to graduate under his supervision.
- Peter Ertl for his excellent scientific support, career consultation and his outstanding approach to motivate and push forward young scientists to be able to reach their full potential.
- Georg Wieselthaler and Shuvo Roy for inviting me to their research group at UCSF - Mission Bay and giving me the opportunity and all the necessary academic and organizational support in order to prove myself during my stay.

It was a great pleasure and a very instructive experience to be part of this project.

Tibor Wladimir

Abstract

The aim of this work was to develop and evaluate a titanium-dioxide coated implantable biosensor for assesing transplant rejection in order to overcome limitations of the state of the art rejection monitoring method. This novel method is based on established contactless bioimpedance sensing to detect tissue changes during the early rejection process. The sensor is implemented at the time of transplant and allows a continuous monitoring with the use of state of the art wireless data transfer. It was demonstrated that our sensor with an electrically insulating titanium dioxide passivation layer in a tetrapolar setup was able to sense morphological changes that may occur during the process of organ rejection. As a proof of concept, whole chicken heart tissue samples were monitored during various degradation processes. The amount of decrease in reactance at a frequency of 5 kHz may be a straightforward and effective method to detect and monitor acute and chronic cardiac allograft rejection without any additional surgical invasive treatment. This work hopes to offer a first insight in bioimpedance based cardiac graft rejection monitoring and thus make a small contribution to developing an implantable biosensor, that might replace endomyocardial biopsies permanently.

Keywords: Passivated Tissue Impedance Spectroscopy, Cardiac Graft Rejection, Non-invasive Monitoring, Biomedical Instrumentation

Zusammenfassung

Das Ziel dieser Arbeit war es einen Titandioxid beschichteten implantierbaren Biosensor für die Überwachung von Abstoßungsreaktionen im Herzgewebe zu entwickeln, um die aktuelle Methodik der Überwachung nach Stand der Technik zu verbessern. Dieses neuartige Verfahren basiert auf einer etablierten kontaktlosen Bioimpedanzmessung und versucht Gewebeänderungen während der frühen Abstoßung im Gewebe zu detektieren. Der Sensor soll zum Zeitpunkt der Operation implementiert werden und ermöglicht eine kontinuierliche Überwachung des Transplantats mit dem Einsatz von modernster drahtloser Datenübertragung. Es wurde gezeigt, dass morphologische Veränderungen während der Abstoßung mithilfe eines durch Titanium Dioxid passivierten Sensors, in einem tetrapolaren Aufbau detektiert werden können. Eine Abnahme des imaginären Reaktanzsignals bei einer Frequenz von 5 kHz scheint ohne zusätzliche chirurgisch-invasive Behandlung eine einfache und effektive Methode für die Erkennung und Überwachung von akuten und chronischen Herzabstoßungsreaktionen zu sein. Der Autor hofft mit dieser Arbeit einen ersten Einblick in die bioimpedimetrische Herztransplantatabstoßungsüberwachung zu bieten und damit einen kleinen Beitrag zur Entwicklung eines implantierbaren Biosensors zu leisten, der auf lange Sicht endomyikardiale Biopsien dauerhaft ersetzen kann.

Stichwörter: Impedanzspektroskopie im Herzgewebe, Transplantabstoßung, Nichtinvasive Patientenüberwachung Monitoring, Biomedizinische Instrumente

Contents

List of Figures

List of Tables

Nomenclature

Acronyms

AC	Alternating Current
BLM	Bilayer lipid membran
CNC	Computer Numerical Control
CPE	Constant Phase Element
CV	Cyclic Voltammetry
DC	Direct Current
EDTA	Ethylenediaminetetraacetic acid
EMB	Endomyocardial Biopsy
HLA	human leukozyte antigen
ISHLT	International Society for Heart and Lung Transplantation
IUPAC	International Union of Pure and Applied Chemistry
MHC	major histocompatibility complex
MPTMS	(3-mercaptopropyl)trimethoxysilane

PBS Phosphate Buffered Saline

PDMS Polydimethylsiloxane

rcf relative centrifugal force

SI International System of Units

TiO_x titanium dioxide

Ti Titanium

Greek Symbols

ϵ Relative permittivity

ϵ_0 Permittivity of vacuum

ϵ_r Permittivity of material

κ cell constant

Ω ohm

ω Radial Frequency

ϕ Phase Shift

δ viscosity

μ mobility

ν drift velocity

σ Conductivity

f Frequency

π	$\simeq 3.14\ldots$

Roman Symbols

c	Concentration
e	elementary charge
l	length
λ	Sensitivity
S	Cross sectional area
z	ion valence
A	ampere
B	Suspectance
C	Capacitance
G	Conductance
I	Current
J	Electrical current density
R	Resistance
V	Voltage or volt
Y	Admittance
Z	Impedance

1 Introduction

Heart failure is the largest cause of hospitalization and death in developed countries, as shown in Figure 1.1 and Table 1.1 and one of the leading causes of disease burden in developing countries [Johnson et al., 2014; Bui et al., 2011]. The reason for that in many cases are beside congenital defects, factors that can be derived from an unhealthy lifestyle such as stress, excess of weight, smoking and above-average alcohol consumption [Nyberg et al., 2013]. For many of those patients, there is no other option left, but to undergo a heart transplantation[1] [Christie et al., 2012]. As shown in Figure 1.2, since the early 1990s, the number of cardiac transplantation has plateaued to an annual rate of about 4.000 surgical interventions per year[2] [Lund et al., 2016].

Since the first human-to-human heart transplant operation was performed in 1967 by Christiaan Barnard at the Groote Schuur Hospital in Cape Town, the survival for heart transplant patients has improved over time, mainly due to improved survival

[1] lat. *transplantare* = to graft, to relocate in a medical sense is the act of relocating cells, tissues, or organs (e.g. heart, liver, kidney, lung or pancreas) from one donor to another or from a donor site to another location on the same individuel to substitute or correcting the patient's defective or lacking organ and has been established as a routine medical treatment nowadays.

[2] The presented data includes only the heart transplants that are reported to the ISHLT Transplant Registry. As such, the amount of heart transplant surgeries may be even higher (estimated 44 percent higher) on a worldwide scale

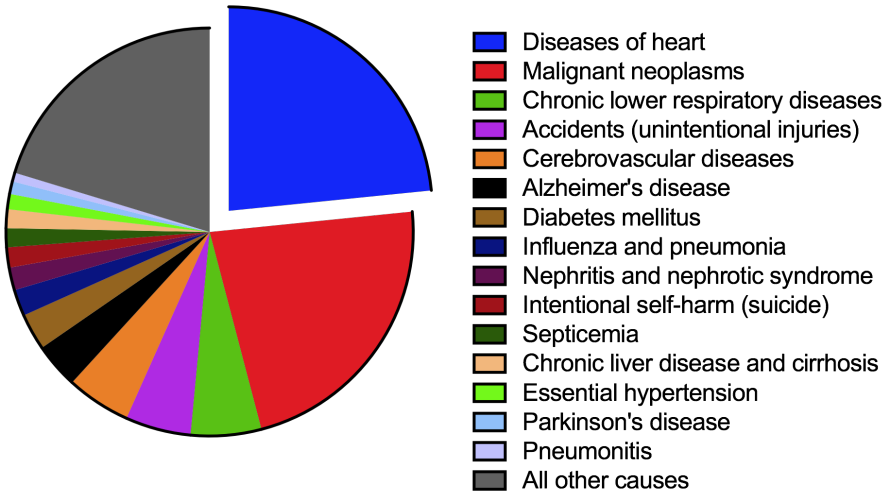

Figure 1.1: Percentage of deaths per 100,000 population in the United States in 2014 by leading cause of death [Kochanek, 2016].

in the early post-transplant period and achievements in immunosupression agents and antirejection medications [Barnard, 1967]. However, the first months following surgery are still crucial to the patient's healing process. Despite all the efforts of modern medicine, heart graft rejection is still an important cause of death in patients with cardiac transplantation. One particular difficulty for a successful therapy is that the patient usually remains asymptomatic until a significant myocardial damage results in heart failure so that about 19 percent of the recipients die within a year of the operation. Thereafter the mortality rate stays constant, at about 4 percent a year for the next 18 years, so that only about 30 percent of patients can expect to be alive after 18 years [Lund et al., 2016].

The endomyocardial biopsy (EMB) is still the gold standard method of investigation for both diagnosing and monitoring many primary and secondary cardiac conditions and among other things to follow allograft rejections after heart transplantation. This invasive procedure percutaneously obtains a sample of the myocardial tissue under investigation, which then can be sent for histological examination. Although a safe

Table 1.1: Number of deaths and percentage of total deaths for the 15 leading causes of death for the total population in 2014: United States [Kochanek, 2016].

Rank	Cause of death	Number	%
...	All causes	2,626,418	100
1	Diseases of heart	614,348	23.4
2	Malignant neoplasms	591,700	22.5
3	Chronic lower respiratory diseases	147,101	5.6
4	Accidents (unintentional injuries)	135,928	5.2
5	Cerebrovascular diseases	133,103	5.1
6	Alzheimer's disease	93,541	3.6
7	Diabetes mellitus	76,488	2.9
8	Influenza and pneumonia	55,227	2.1
9	Nephritis, nephrotic syndrome and nephrosis	48,146	1.8
10	Intentional self-harm (suicide)	42,826	1.6
11	Septicemia	38,940	1.5
12	Chronic liver disease and cirrhosis	38,170	1.5
13	Essential hypertension and hypertensive renal disease	30,221	1.2
14	Parkinson's disease	26,150	1.0
15	Pneumonitis due to solids and liquids	18,792	0.7
...	All other causes	535,737	20.3

method[3], endomyocardial biopsies are clearly associated with both a risk of procedural (e.g. hematoma, pneumothorax, hemothorax, cardiac perforation, arrhythmias, and conduction abnormalities) and long-term complications [From et al., 2011]. On the other hand, their unavoidable necessity after the first posttransplant year and their frequency[4] early after surgery have already been questioned [Sethi et al., 1995; White et al., 1995; Dandel et al., 2001]. Heart transplant patients undergo repeated endomyocardial biopsy procedures during a prolonged period after surgery and are therefore at even a higher risk of long-term complications of the biopsy (e.g. acute rejection, infection, transplant vasculopathy, metabolic complications, renal insuffi-

[3]The rate of complication during endomyocardial biopsies is reported as less than 6% in most case series [From et al., 2011].

[4]The frequency of surveillance biopsy varies among centers. In general, routine endomyocardial biopsies are performed weekly for the first month, then every two weeks during the second month, and increased to monthly through months 8 to 12. After one year, biopsies are done every four to six months.

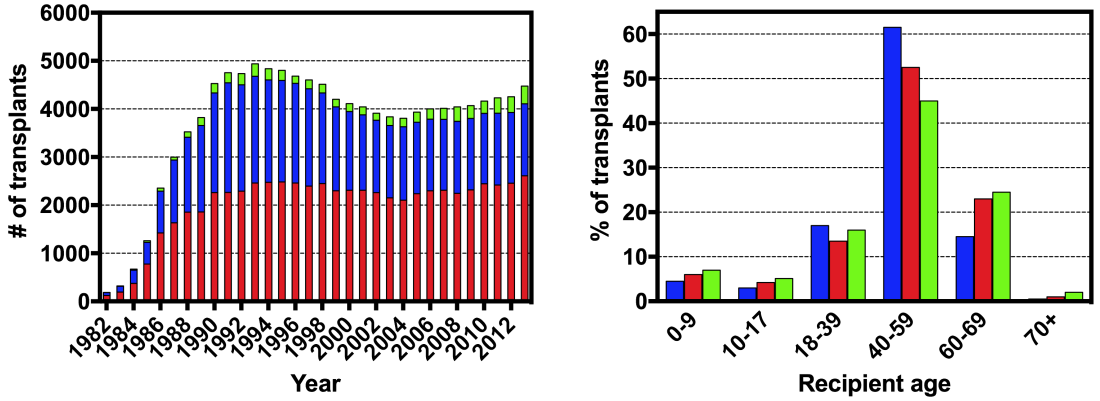

(a) **(b)**

Figure 1.2: Adult and pediatric heart transplants statistics. Selected years, 1982 trough 2012. **(a)** The number of adult and pediatric heart transplants, by year and location (red: North America, blue: Europe and green: others) and **(b)** Recipient age distribution (adult and pediatric) by era (blue: 1982-1995, red: 1996-2005 and green: 2006-2013). Adapted from "The registry of the international society for heart and lung transplantation: Thirty-first adult lung and heart-lung transplant report - 2014; Focus theme: Retransplantation" by Lund et al. [2016], *Journal of Heart and Lung Transplantation 33*, p. 998. Copyright 2014 by ISHLT.

ciency, bone diseases, and malignancy). Beside all the medical risk and a considerable psychological strain on the part of patients, these procedures are also time and cost demanding on the part of the health insurence and healthcare professionals [From et al., 2011].

1.1 Motivation for Development

The importance and benefits of an early therapy to increase the chances of successfully curing patients is unquestioned. To initiate a successful and cost-effective therapy at the early stage, the diagnosis of a rejection must be made before clinical features of cardiac failure occur. Time-resolved and continuous monitoring of implants is vital for early detection and monitoring of events leading to graft rejection and failure. During organ rejection several cellular and humoral processes take place over a pe-

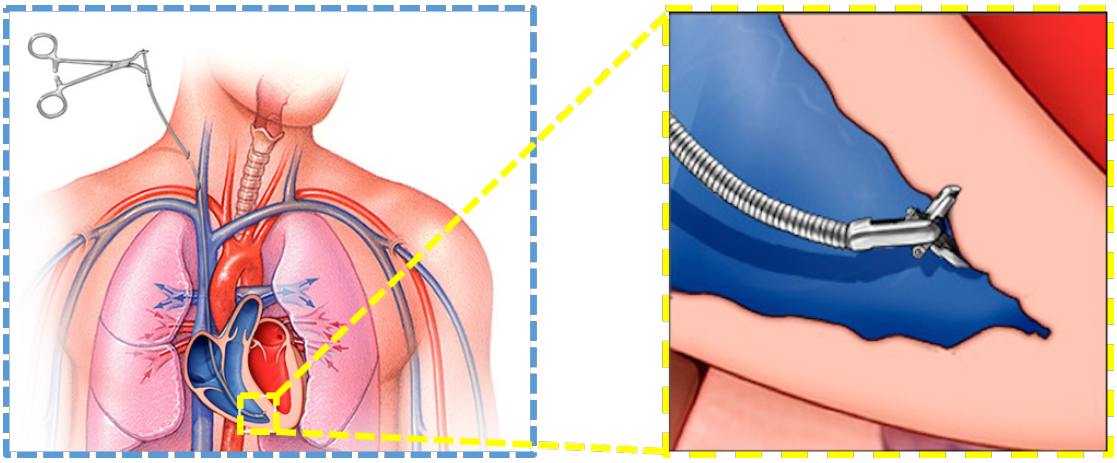

Figure 1.3: Schematic representation of an endomyocardial biopsy procedure. Source: mayoclinic.org

riod of several weeks and months including inflammatory infiltrate of immune cells, cardiac allograft vasculopathy and cytomegalovirus infection [Costello et al., 2013]. Early detection of structural changes in the myocardial tissue can therefore increase the rate of implant success, since early drug administration can reduce morbidity resulting from implant failure. For instance, Basiliximab and Daclizumabis are used frequently to counteract the immune response during cellular rejection [Martin et al., 2015]. Therefor, a full implantable device for continuous, long-term monitoring of morphological changes in cardiac allografts would be a long-desired improvement in transplantation medicine, since both direct costs to healthcare systems and indirect costs to society through morbidity and lost productivity are enormous [Cook et al., 2014; Kittleson et al., 2017].

Development in recent years has led to an overall increase in label-free technologies in biomedical research, where time-resolved measurements are used to quantify phenotypic changes of cells and tissue by monitoring biomolecular interactions without the drawbacks of conventional labelling technologies such as autofluorescent, spatial-interference or quenching effects [Sticker et al., 2015]. Current biosensing

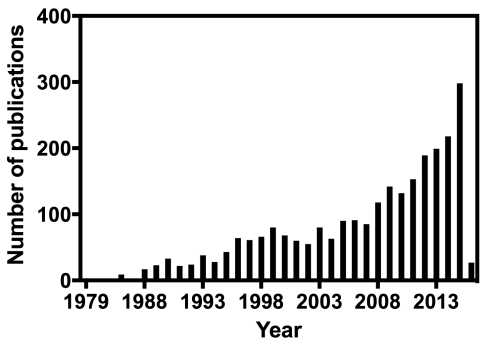

Figure 1.4: This graph shows the number of publications with the keyword 'bioimpedance' per year from 1979 to 2016. The increase shows an exponential trend that will produce nearly 500 bioimpedance publications per year by 2020.

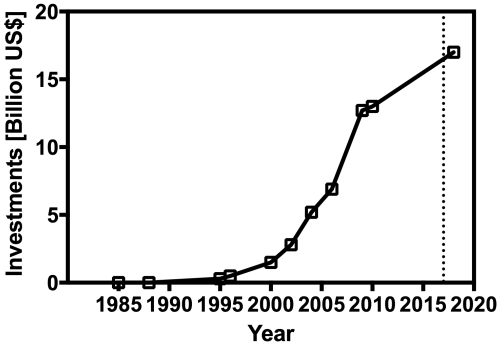

Figure 1.5: Estimated past, present, and future world market for biosensors. Adapted from "Biosensors: then and now" by Turner [2013]. Current year marked by a dashed line.

technologies have become an integral part of everyday life, providing highly accurate, sensitive diagnostics. These applications are of increasing prominence in healthcare, agriculture, food industry, environmental and security sectors, hence this is reflected in the continuously increasing growth of global markets for such technologies, as seen in Figure 1.5. In particular with regard to the biosensor market, where today after a phenomal growth since the 1985s the worldwide sales of biosensors are worth of about US$ 13 billion [Turner, 2013].

To overcome limitations of the state of the art rejection monitoring methods, the proposed project sets out to develop and evaluate titanium-dioxide coated implantable biosensors for transplant rejection monitoring. This novel method is based on established contactless bioimpedance sensing to detect tissue changes on morphological tissue integrity during the early rejection process. The sensor will be implemented at the time of transplant and allows a continuous monitoring with the use of state of the art wireless data transfer.

Over the last decades many clinical and non-clinical applications have been estab-

lished using bioimpedance and bioelectricity. Electrical impedance measurements have been adapted for tissue characterization and cell behaviour studies [Reza Atefi et al., 2013; Prodan et al., 2004; Sun et al., 2010], body composition and intra/extracellular fluid index as well as heart and respiration rate can be determined for monitoring nutrition and physical training in sport medicine [Galanti et al., 2015] and meat quality and fermentation can be followed in food and beverage industry [Wang et al., 2012] but also applications in stem cell differentiation monitoring [Frazier et al., 2009; Hildebrandt et al., 2010; Reitinger et al., 2012], cytotoxicity screening [Ju and Park, 2005; Xiao and Luong, 2003], cell spreading [Wegener et al., 2000] and IgE-mediated mast cell activation [Abassi et al., 2004] have been introduced. As shown in Figure 1.4, the rate of growth in scientific publications on bioimpedance proves the current importance of this research field and its impact on the future of academic research in the upcoming years.

1.2 Research Goals

Thus, the research goal of this work is on one hand the confirmation of the hypothesis that physiological changes in cardiac muscle tissue during organ rejection can be detected by a measurement of the electrical bioimpedance, on the other hand the developing of an implantable prototype for early detection and monitoring of cardiac tissue degeneration based on tissue impedance spectroscopy, that can be used in further research. As mentioned before, studies have shown that contactless bioimpedance sensing is particularly sensitive towards cell morphology changes, tissue remodeling events and cell movements and thus also ideally suited to detect the invasion of lymphocytes into the transplant and early oedema and cell necrosis, which are all known processes that occur during transplant rejection. Therefore, it has been

specifically investigated whether titanium electrodes with an electrically insulating titanium dioxide passivation layer in a tetrapolar setup could be used to detect the morphological and structural changes in tissue, that may occur during the process of organ rejection.

2 Theoretical Background

The following chapter deals with the necessary theoretical background information to both the biological background of tissue rejection and the concept of bioimpedance based biosensing.

2.1 Biology of Transplant Rejection

2.1.1 Types of Grafts

The extent of an immune response and thus the extent of rejection to an implant primarily depends on the degree of genetic variation between host and receiver. There are mainly four types of grafts: (1) xenografts, which are transplants between different species, (2) allografts, which are grafts between genetically differentiated members of the same species, (3) autografts, which are transplanted from one to another part of the body (e.g. skin grafts) and (4) isografts, which are transplants between genetically indentical individuals such as identical twins. Consequently, in the first case we expect the highest immune response leading to a rapid graft rejection, in contrast to isografts, that undergo no immune response and therefore no rejection at all. Secondly, the type

and degree of immune response vary also with the type and site of an implant. While grafts concerning the eye or brain have minimal or no immune cells and therefore tolerate even mismatched implants, highly vascular organs such as the human heart, liver or kidney lead to an intense and powerful host response [Kindt et al., 2007].

2.1.2 Mechanisms of Rejection

The immune system has developed many effective mechanisms to fight foreign objects invading our body that are also involved in the rejection of transplanted organs. These processes consist of both humoral antibody-mediated and cell mediated cytotoxicity mechanisms and are based on an antigen recognition process involving especially T-cells and B-cells with the responsible antigens called major histocompatibility complex (MHC) or human leukozyte antigen (HLA) in human. In case of mismatching AB0[1] compatibility the graft is rejected immediately after implantation due to preexisting anti-HLA antibodies in transplant recipient, otherwise the graft rejection occurs in two stages: (1) a sensitization stage and (2) an effector stage [Kindt et al., 2007].

Sensitization Stage of Graft Rejection

During the sensitization stage, T cells recognize alloantigens exposed on the surface of the implants by either recognizing the donor MHC molecule directly (direct pathway) or through the recognition of peptides of the donor HLA presented on the surface of the recipients APCs (indirect pathway). If an APC expresses an antigenic-ligand/MHC molecule and provides a costimulatory signal, a T helper cell gets activated leading to a more severe immune response in the patient [Kindt et al., 2007].

[1] The AB0 system is the major human blood group system based on the proteins on the surface of erythrocytes.

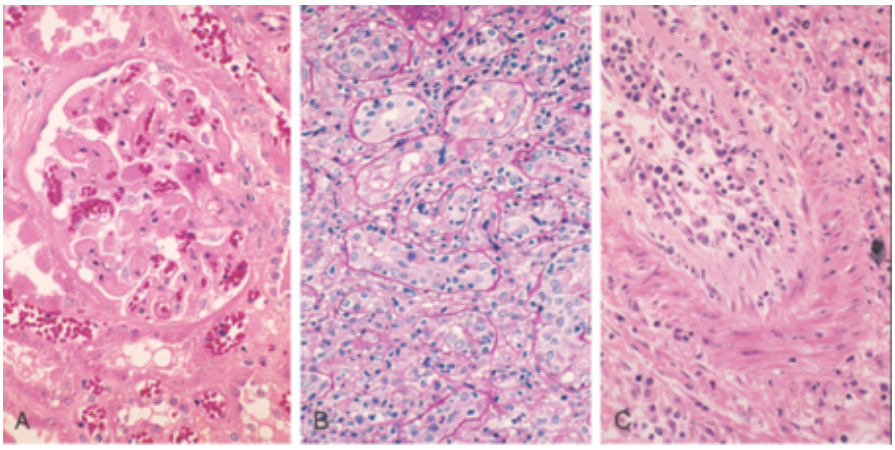

Figure 2.1: Clinical stages of graft rejection. **A** hyperacute graft rejection, **B** acute cellular rejection and **C** acute humoral rejection. Adapted from "Pathologic Basis of Disease, 8th Edition" by Kumar et al. [2009], Copyright 2009 Elsevier, Inc.

Effector Stage of Graft Rejection

In the effector stage the immune destruction of the implant occurs. The most common mechanisms are cell-mediated reactions involving an influx of immune cells such as CD4+, APCs or macrophages into the graft, that will lead to cell morphology changes and tissue remodeling and therefor to structural changes due to apoptosis of myocardial cells of the graft [Kindt et al., 2007].

2.1.3 Clinical Stages of Rejection

We can define three different clinical stages of rejection: (1) hyperacute rejection, (2) acute rejection and (3) chronic rejection as shown in Figure 2.1. In principal, we can say that rejection in solid organ transplantation is presented as an immune-mediated process of morphological tissue alteration (e.g. lymphocyte invasion, cell swelling, ischemia, edema, fibrosis, necrosis) which ends in loss of organ function. Results of these tissue alteration processes should be detected in very early stages to improve treatment in cardiac transplantation.

Table 2.1: Overview about the existing applications using impedance

Type of Measurements	Analysis methods	References
Cellular Measurements	Coulter counter	[Wu et al., 2011]
	Measurements of the hematocrit	[Trebbels et al., 2009]
	Monitoring cell cultures	[Bragós et al., 1999]
Volume Changes	Impedance plethysmography	[Ferreira et al., 2013]
	Impedance cardiography	[Cybulski et al., 2012]
	Impedance pneumography	[Młyńczak and Cybulski, 2012]
Body composition	Fluid compartments	[Jaffrin, 2009]
	Fat compartments	[Vine et al., 2011]
Tissue monitoring	Ischemia monitoring	[Ahn et al., 2005]
	Graft viability assessment	[Khalil et al., 2014]
	Graft rejection monitoring	[Giovinazzo et al., 2011]
Tissue classification	Electrical Impedance Spectroscopy	[Dean et al., 2008]
	Electrical Impedance Tomography	[Costa et al., 2009]

2.2 Fundamentals of Bioimpedance

People have been fascinated with electricity for many centuries like with no other technological invention in history[2]. It was Luigi Galvani (1737-1798) who first proved in his frog experiments at the university of Bologna, that the living body utilises electricity to control muscle movement [Galvani, 1791]. A few decades later Oliver Heaviside (1850-1925) coined amongst many other things the term "impedance" in the form we use today. About the same time, measurement of electrical conductance in human skin began and became the precursor of the lie detector. Around 1905, the electric galvanometers were sensitive and rapid enough for heart activity measurements, and, by 1910, Rudolf Höber (1873-1953) used bioimpedance to prove the existence of cell membrans [Höber, 1910]. In order to show the potential of this technique, Table 2.1 provides an overview about the existing applications.

[2] A complete historical retrospective review is available in Grimnes and Martinsen [2015].

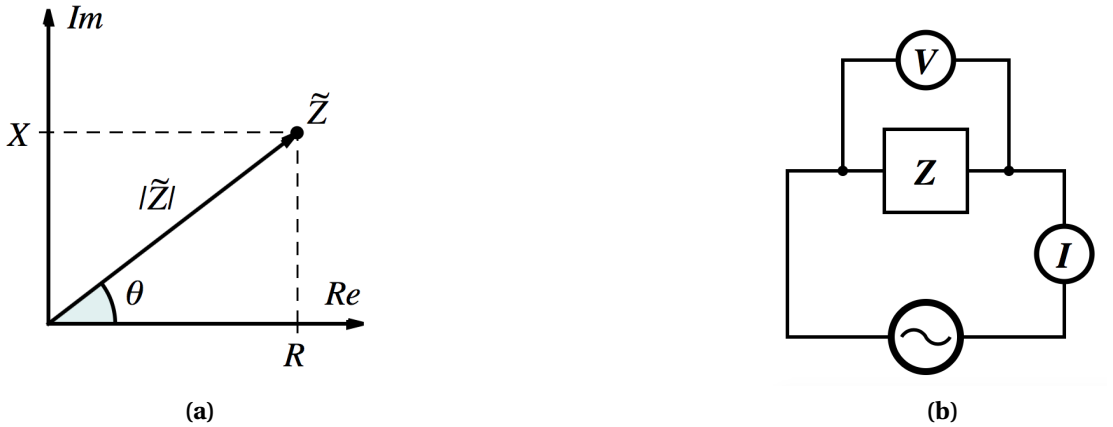

Figure 2.2: A graphical representation of the **(a)** complex impedance plane, where X is the reactance, R the resistance and ϕ the phase shift and **(b)** a basic impedance circuit consisting an AC supply applying a voltage V driving a current I.

2.2.1 Essential Electrochemical Basics

Bioimpedance[3] (Z) refers to the passive electrical properties of a biological tissue, measured by applying an alternating current potential (AC) to the tissue externally and then measuring the electric current (I) through it. According to Ohm's law (2.1), the ratio between voltage V in units of volts [V] and current I in units of amperes [A] remains constant, if temperature and all other factors remain constant. This ratio is called "resistance" and is abbreviated by the roman letter R. The SI unit of resistance is the ohm [Ω].

$$R = \frac{V}{I} = const. \tag{2.1}$$

Due to its limitation by simplifying properties, Ohm's law only applies to the ideal resistor. To describe more complex behaviour such as the electrical properties of a biological tissue, we use impedance as a more general parameter and complex quantity. The excitation signal, that is used to measure an electrochemical impedance,

[3]The word *"impedance"* comes from the Latin word *"impedīre"* to hinder, literally, to shackle the feet, from *pedīre*, v. derivative of *pēs* foot

can be expressed as a function of time, that has the form

$$V_t = V_0 \sin(\omega t) \tag{2.2}$$

where V_0 is the amplitude of the signal, ω is the radial frequency and V_t is the potential at time t. The relationship between radial frequency ω and frequency f is:

$$\omega = 2\pi f \tag{2.3}$$

The response signal I_t is shifted in phase ϕ in a linear system and has a different amplitude than I_0.

$$I_t = I_0 \sin(\omega t + \phi) \tag{2.4}$$

Thus, in accordance with Ohm's Law the impedance results in:

$$Z = \frac{V_t}{I_t} = \frac{V_0 \sin(\omega t)}{I_0 \sin(\omega t + \phi)} = Z_0 \frac{\sin(\omega t)}{\sin(\omega t + \phi)} \tag{2.5}$$

Using Eulers relationship,

$$\exp(j\phi) = \cos\phi + j \sin\phi \tag{2.6}$$

the potential can be described as,

$$V_t = V_0 \exp(j\omega t) \tag{2.7}$$

and the response current as,

$$I_t = I_0 \exp(j\omega t - \phi) \tag{2.8}$$

Thus, the impedance is then described as a complex number by using Eulers relationship again,

$$Z(\omega) = \frac{V}{I} = Z_0 \exp(j\phi) = Z_0(\cos\phi + j\sin\phi) \tag{2.9}$$

or

$$Z = R + jX \tag{2.10}$$

where the real component of impedance is the resistance R and the imaginary component is the reactance X following equation,

$$Z = \sqrt{R^2 + \frac{1}{(2\pi f C)^2}} \tag{2.11}$$

where, C is the capacitance. For a better understanding, impedance functions are often depicted in a graphic form, as noted in Figure 2.2. Another often used expression is the reciprocal of the impedance called admittance and is abbreviated by the roman letter Y in Siemens.

$$Y = G + jB = G + j\omega C \tag{2.12}$$

where in a similar form to real and imaginary impedance, G is the conductance and B is the suspectance of the admittance.

2.2.2 Impedance Spectroscopy of Electrolytes

The electric current in metals and consequently in electrodes is carried by electrons. In electrolytes on the other hand, the charge transfer takes place by ions and other

Table 2.2: Approximate concentration of electrolytes in body liquids (meq/L) is ion concentration in milliequivalents (mmole × valency z) per Liter. Data from Grimnes and Martinsen [2015]

Cations (meq/L)			**Anions (meq/L)**		
	Plasma	**Intracellular**		**Plasma**	**Intracellular**
Na^+	142	10	Cl^-	103	4
K^+	4	140	$HCO_3{}^-$	24	10
Ca^+	5	10^{-4}	Protein	16	36
Mg^+	2	30	$HPO_4{}^{2-}$ + $SO_4{}^{2-}$ + organic acids	10	130
H^+ (pH = 7.4)	4×10^{-5}	4×10^{-5}			
Sum	153	180	Sum	153	180

0.9% NaCl is 154 mmol/L.

charged molecules that are able to migrate in a solvent. Thus, charge movement under the influence of an electrical field appears in electrolytes in both directions with the existence of a positive type (cation) and a negative type (anion) of charge carriers [Sticker et al., 2015]. The flow velocity of these ions can be described by Ohm's Law for electrolytes,

$$\nu = \mu \mathrm{E} = \frac{ze}{6\pi\delta R_e f f} E \tag{2.13}$$

where ν represents the drift velocity, μ the mobility, z the ion valence, e the elementary charge and δ the viscosity of the surrounding medium. As a simplification, in small ion concentrations or by small concentration changes in charged molecules, a linear relationship between conductance and concentration can be assumed. Thus, the electric current per area of an electrolyte, called as electrical current density J (2.14) is proportional to the conductivity σ and to the amount of ions n.

$$\mathrm{J} = \sigma \mathrm{E} = nze\mu E \tag{2.14}$$

Table 2.3: Electrical resistivity in biological material. Adapted from Geddes et al. [Geddes and Baker, 1967].

Type of tissue	Resistivity [Ω cm]
Blood plasma	63
Blood (for hematocrit Ht = 47 %	150
Skeletal muscle (longitudinal)	300
Skeletal muscle (transverse)	700
Cardiac muscle (dog)	750
Lungs (dog)	1,200
Fat	2,180
Saline 0.9 %	57

During measurement of conductivity a so-called electrical double layer [Bard and Faulkner, 2002] occurs at the electrode/electrolyte interface causing an additional resistance that has been described with different models in the literature by several authors [Bohinc et al., 2012; Oldham, 2008; McAdams et al., 1995]. The so-called Warburg model (2.15) has been found widespread use and states that the electrochemical response is dominated by pure diffusion of the active species.

$$Z_w = (1-j)\sigma\omega^{-\frac{1}{2}} \tag{2.15}$$

However, to avoid a complex system and and discharges with the electrode surface, electrodes should be covered with dielectrics to minimize the additional resistance caused by this electrical double layer [Sticker et al., 2015].

2.2.3 Electrical Properties of Tissue

The electrochemical properties of biological tissues and cell suspensions are mainly given due to the capacitive reactive behaviour of the highly insulating plasma membran of the cell build by a phospholipid bilayer as shown in Figure 2.3 and the resistive behaviour based on the composition such as electrolyte concentration, carbohydrates,

membrane composition [Grimnes and Martinsen, 2015]. However for simplification from the electrical point of view, it is generally accepted that biological tissue behave as a complex anisotropic conductor, where the current is transported by ions[4] in the intra- and extracellular space [Grimnes and Martinsen, 2015]. The extent of the reactive and resistive behaviour of the tissue depends on the applied frequency. As shown in Figure 2.4 at low frequencies ($f \to 0$) most of the current flows around the cell without being able to penetrate into the cell [Grimnes and Martinsen, 2015]. At high frequencies ($f \to \infty$) the membrane capacitance is no impediment to the current and it flows indiscriminately trough the extra- and intracellular media [Ivorra, 2013]. This becomes even more obvious by looking at (2.11), so that if $f \to \infty$, the resistance term will be dominating. This impedance varies not just with altering frequency (f) but also with different tissue types and changes sensitively with the underlying histology of the investigated tissue [Grimnes and Martinsen, 2015]. This characteristics can be used on one hand to differentiate between different tissue types and on the other hand in order to detect pathological changes in tissue. Based on the data presented in Table 2.3, it can be assumed, that a change of impedance in a biological tissue is attributed to an altering composition within the tissue due to a pathological modification such as ischemia, edema or cell migration [Geddes and Baker, 1967]. Schwan et. al emphasized in his work the importance of specific frequency regions for the dielectric properties in biological materials as seen in Figure 2.5 [Schawn, 1957]. However only α and β dispersion with their frequency range < 10 MHz are particularly interesting for this application, since most changes between normal and pathological tissue seem to appear in this frequency range [Blad and Baldetorp, 1996]. In general, α dispersion is associated with diffusion processes of the ionic species at lower frequencies, β dispersion on the other hand is linked to the dielectric properties of the

[4]The most important ions are listed in Table 2.2 [Grimnes and Martinsen, 2015].

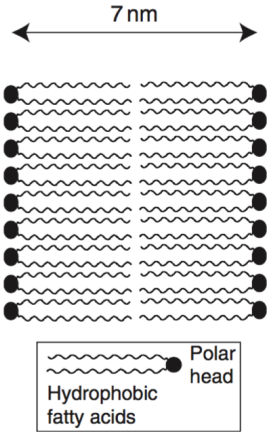

Figure 2.3: Bilayer lipid membran (BLM), the main component of the cell membrane. Due to the ion concentration gradient between the inside and outside of the cell and the membrane proteins embedded in the membrane, the cell surface is charged negatively. Reprinted from "Bioimpedance and Bioelectricity Basics" by [Grimnes and Martinsen, 2015], p. 101. Copyright 2015 by Elsevier Ltd.

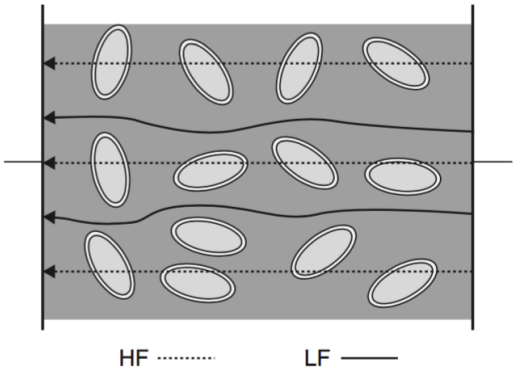

Figure 2.4: Low and high frequency current paths in tissue. Current flows through the path of least resistance, so at low frequency (LF), the current flows mainly between the cells, only by increasing frequency it is able to penetrate the cell. Reprinted from "Bioimpedance and Bioelectricity Basics" by [Grimnes and Martinsen, 2015], p. 103. Copyright 2015 by Elsevier Ltd.

bilayer lipid membran and other internal membrane structures. Some other physical properties such as temperature or pH value contribute to changes in impedance to a certain degree. Since the viscosity decreases with rising temperatures, according to (2.13) the resistance of a solvent decreases due to an increasing ionic mobility. The pH value under physiological conditions[5] varies between pH 6-8 and does not contribute significantly due to the very low concentration of H_3O^+.

2.2.4 Theoretical Cell Constant

Beside the electrical properties of a tissue such as conductance and suspectance, impedance values are also determined by the geometrical constrains. Grimmnes et al. have defined a geometrical scaling factor κ that allows the comparisment of different

[5]Physiological condition, in a medical sense, is a number of physiological values used to describe the conditions that occur in humans such as atmospheric oxigen concentration, temperature range of 20 to 40 degrees Celsius, pH 6-8 etc.

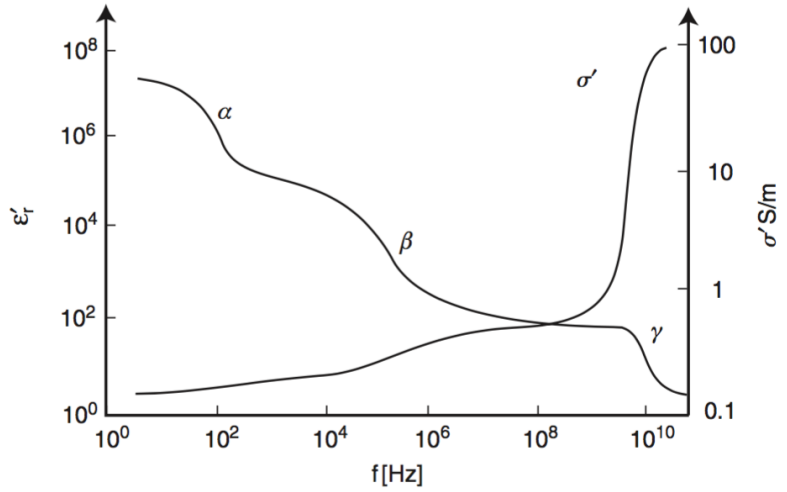

Figure 2.5: Idealised dispersion regions for tissue. On the one hand α dispersion is associated with diffusion processes of the ionic species, on the other hand β dispersion is linked to the dielectric properties of the bilayer lipid membran and other internal membrane sturcures. γ dispersion, caused by molecules and proteins in aqueous solution, can be ignored since they only appear at higher frequencies. Adapted from "Bioimpedance and Bioelectricity Basics" by [Grimnes and Martinsen, 2015], p. 103. Copyright 2015 by Elsevier Ltd.

sensors based on their dimensions [Grimnes and Martinsen, 2015].

$$\kappa = \frac{S}{l} \tag{2.16}$$

where, S is the cross sectional area of a tissue under observation and l the length of the measuring electrodes. Thus, in accordance with (2.12) the admittance results in:

$$Y = G + jB = G + j\omega C = \kappa(\sigma + j\omega\epsilon) = \kappa(\sigma + j\omega\epsilon_r\epsilon_0) \tag{2.17}$$

where ϵ_r is the permittivity of the material and ϵ_0 is permittivity of the vacuum.

2.2.5 Equivalent electrical circuit for biological tissue

Considering the electrical properties of a biological tissue and applying the theory of electrical circuits, a simplified equivalent electrical model for the cell can be shown in

Figure 2.6. As mentioned before, the current can flow trough the cell across the phospholipid membran (C_m) or across the ionic channels (R_m) or can circulate around the cell (R_e). Once the current penetrated the cell, it moves trough the intracellular medium (R_i) and leaves the cell across the membrane ($R_m \parallel C_m$). Usually, the membrane conductance (R_m) is very low and can be ignored [Ivorra, 2013]. Since

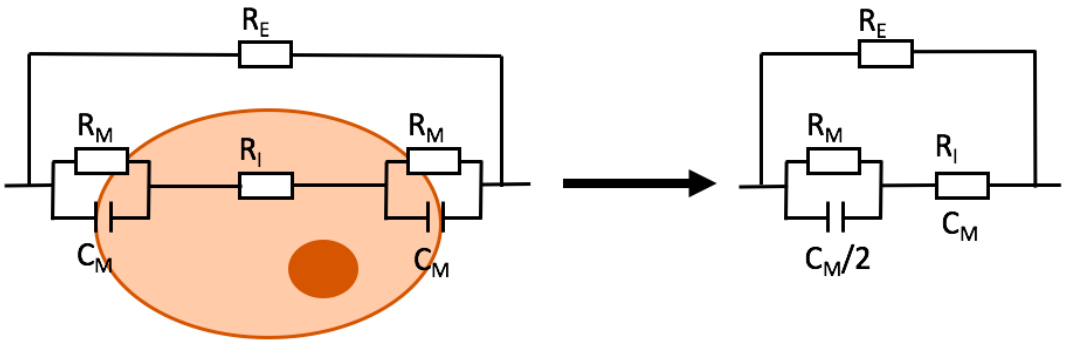

Figure 2.6: Simplified equivalent electrical circuit for biological tissue, where R_e is the extracellular fluid Resistance, R_i is the intracellular fluid Resistance, R_m is the trans-membrane ionic channel Resistance and C_m represents the cell membrane capacitance. Adapted from "Bioimpedance Monitoring for Physicians: An Overview." by Ivorra [2013], p. 19. Copyright 2003 by Centre Nacional de Microelectrònica Biomedical Applications Group

a biological material is not homogeneous and cell sizes are randomly distributed, a more detailed model is needed. Cole et al. suggested a more realistic model for tissue, where the capacitor is substituted by a Constant Phase Element (CPE) and the phase is frequency independent [Cole, 1940].

Hence, CPE has the impedance:

$$Z_{CPE} = \frac{1}{(j\pi f C)^{\alpha}} \tag{2.18}$$

where j is the imaginary unit, f the frequency, C the capacitance. The CPE parameter α, that takes a value between 0 and 1, allows to describe different spectral shapes

Ivorra [2013]. When $\alpha = 0$, the behavior of the CPE is exactly the same of an ideal capacitor, when $\alpha = 1$ the CPE behaves like an ideal resistor. Substituting R_m and C_m with CPE in the circuit in Figure 2.6 results in

$$Z_{CPE} = R_\infty - \frac{R_0 - R_\infty}{1 + (j2\pi f\tau)^\alpha} \tag{2.19}$$

When more than one dispersion occurs, the Cole equation can be expanded:

$$Z_{CPE} = R_\infty - \frac{(R_0 - R_\infty)_1}{1 + (j2\pi f\tau_1)^{\alpha_1}} + \frac{(R_0 - R_\infty)_2}{1 + (j2\pi f\tau_2)^{\alpha_2}} + \ldots \tag{2.20}$$

R_∞ is the resistive part at infinite frequency, R_0 is the impedance at 0 Hz, τ is a time constant. Different tissue samples can be characterized by finding these four parameters[6].

2.2.6 Frequency and Current Values

According to Webster et al. there is a general consensus by using a sinusoidal current with the amplitude between 1 and 5 mA and a frequency between 20-100 kHz in medical applications [Webster et al., 2010]. However, a direct electrical connection to the cardiac muscle and an invasive application of a measuring current to the myocardium requires a high standard of safety, so it is advisable to use as low current as possible. The use of direct current (DC) in biological tissue is very limited due to the fact that it causes chemical changes such as changes in pH and the permeability of the cell membran, distribution of ions when it passes through the cells and intra- and extracellular fluids.

[6] A quantitative analysis of the equivalent electrical circuit is not part of this thesis.

Table 2.4: Classification of transducer

principle	**examples**
potentiometric	ion-selective electrode, soon-selective field-effect transistor
amperometric	metal electrodes, conduction organic salts
acoustic	piezoelectric/surface acoustic wave, bulk acoustic wave
calorimetric	thermometric biosensor
optical	ellipsometry, fibre optic, planar waveguide, surface plasmon resonance

2.3 Biosensors

According to the International Union of Pure and Applied Chemistry (IUPAC), the term "biosensor" is short for "biological sensor" and is a device using a specific biochemical reaction mediated by isolated enzymes, immunosystems, tissues, organelles or whole cells to detect chemical compounds by electrical, thermal or optical signals [Guilbault and Hjelm, 1989]. In general, a biosensor is a measuring system that is composed by a biological recognition element and an physicochemical transducer part. There are different ways that biosensing may occur measuring either the affinity of binding or metabolic and catalytic changes on the surface of the sensoring element. Depending on the task, the biological recognition is performed by a variety of elements such as enzymes, antibodies, microorganisms, organelles or biological tissues. Thus, there are several commonly used technological possibilities for transducer that respond to the products of the biocatalytic or binding process. Table 2.4 categorizes transducers into five main types on the basis of the applied physical principle. A purposeful combination of these elements depends on the analytical problem, which is needed to be answered. Furthermore, a signal processing part is needed, which takes the electrical signal through an integrated system to present data to the operator.

2.3.1 Flexible Electronics

Flexible electronics is a technology in biosensor development for fabricating electronic circuits by attaching electronic devices on flexible plastic substrates. In recent years the focus has been set on this research field for mainly two reasons. Firstly, they promise an entirely new way of engineering electronics allowing flexible, bendable, lightweight design that can be used in medical application, photovoltaic cells and consumer electronics. Secondly, flexible electronics allow a cost-effective production due to high volume manufacturing or by using fewer expensive manufacturing processes. Particularly with regard to our research goal, a flexible sensor is crucial due to the curvilinear surface and the mechanism and contraction events of a cardiac muscle.

Flexible electronic devices can be fabricated by using several different techniques. In general, two basic approach have been used for fabrication: (1) a circuit is produced separately by standard methods on a transfer substrate (e.g. Si wafer, glass plate) and then transferred on a flexible substrate [Lee et al., 2003] or (2) the circuit will be processed directly on a flexible substrate by using additive printing methods [Yin et al., 2010; Khan et al., 2015] and pattern transfer [Du et al., 2012]. A review on different techiques and materials used in this field can be found in [Cheng and Wagner, 2009].

2.3.2 Electrode Material

At the heart of all biosensing systems are the electrodes. Geddes et al. has defined four criteria that should be considered when choosing material for an implanted electrode: (1) tissue response, (2) allergic response, (3) electrode-tissue impedance, and (4) radiographic visibility [Geddes and Roeder, 2003].

Tissue Response

Introducing a foreign object such as a metal implant into a tissue causes essentially two different responses: (1) the surrounding tissue fluid tries to dissolve the implant and (2) following an inflammatory cascade, the body reacts by forming a protective cover around it, called capsule formation. Depending on the material used, a varying thickness may be formed leading to a reduction of the amplitude available for recording measurements [Geddes and Roeder, 2003].

Allergic Response

Needless to say, an ideal implanted electrode may not trigger any allergic response by the host. Therefore, although prima facie some metals are excellent qualified, by adding a nonallergenic criterion for selection reduces the list of suitable metals for an implanted electron. A hierarchy of allergenic metals can be found in [Geddes and Roeder, 2003].

Electrode-Tissue Impedance

Impedance and the influence of tissue characteristics on a bioimpedance measurement have been defined in Chapter 2. In summary, it can be stated, that the impedance of an electrode-electrolyte interface, that can be seen as a simplified system to an electrode-tissue interface, depends on the type of electrolyte it contacts, on the temperature and on the species of metal and its surface area - the larger and rougher the surface, the smaller the impedance [Geddes and Roeder, 2003]. Derived from (2.11) we also can see, that the bioimpedance is clearly frequency-dependent resulting to a decreasing impedance value with increasing frequency used to measure.

Radiographic Visibility

Since our goal is to develop an instrument for a long-time monitoring of the cardiac tissue, we need to consider radiographic visibility as a requirement, so clinician are also able to monitor the integrity and operative readiness of the implant over time. Due to its small size, it is recommended to select a metal with a high atomic number, that absorbs X-rays effectively [Geddes and Roeder, 2003].

3 Materials and Methods

This chapter describes all materials and methods for the development of a prototype of an implantable biosensor for rejection detection and long-term monitoring in cardiac transplantation acquired in scope of this work. Additionally, a complete list of materials can be found in Appendix.

3.1 Selection of Materials

Several criteria according to the flexibility of a sensor have been discussed in Chapter 2. Since the main goal of this research project is the development of an implantable medical application, there are different aspects to consider when choosing a biomaterial[1] for manufacturing biosensors in addition to the essential expectation of functional ability, flexibility (e.g. biocompatibility[2], availability, costs of raw materials etc.). Since the developed sensor is intended to detect and monitor rejection of an implant over a long period of time, a highly tolerable and biocompatible material is needed. Based

[1] Biomaterial in medical terminology is *"any natural or synthetic material that is intended for introduction into living tissue especially as part of a medical device or implant"* [Bhat and Kumar, 2013]

[2] The International Union of Pure and Applied Chemistry (IUPAC) defines the term biocompatibility as *"the ability to be in contact with a living system without producing an adverse effect."*[Vert et al., 2012]

on the criteria discussed in Chapter 2 and its widespread and successful application in medical implants [Ratner et al., 2008; Balazic et al., 2007; Liu et al., 2004], a titanium (Ti) electrode with an insulating titanium dioxide surface has been selected for further development.

PDMS[3] is well known for its flexible properties and is has been used in implantable devices for long term studies already [Kim et al., 2011]. Although there is some controversy about whether PDMS is the most appropriate material for implantable devices due to its lacks the ability to be easily functionalized with biologically active components, due to its easy handling and availibility on the other side, it has been chosen as a substrate for our purposes [Domachuk et al., 2010].

Needless to say, that in the end all other materials, that will be used during fabrication such as wires and conductive paste, should meet the same criteria for biocompatibility.

3.2 Electrode Passivation

According to IUPAC, passivation is a process of transition from the active to the passive state by formation of the passivating film, that is achieved by an anodic current which at the respective electrode potential must be larger than the maximum current, by the presence of an oxidized substance in the neighbouring solution which passivates by being reduced or by sufficient heating under normal atmospheric conditions [Heusler et al., 1989] As stated above, titanium is very-well suited for medical applications, due to to its biocompatibility and corrosion resistance. The latter especially comes from the amorphous surface passive oxide layer which consists of mainly TiO_x and provides chemical inertness in many aqueous media [Jamesh et al., 2013]. Sticker et

[3] Polydimethylsiloxane, short PDMS, is a silicon-based organic polymer frequently used in microfluidics.

al. have demonstrated that complete sensor isolation using metal oxide coatings such as titanium dioxide and resulting physical removal of the impedance electrodes from the liquid sensing environment eliminates ohmic (faradaic) contributions, bubble formation and electrode polarization events, thus providing stable and non-drifting measurement conditions over long periods of time [Sticker et al., 2015].

3.2.1 Thermal Oxidation of Titanium

Titanium reacts spontaneously with the atmospheric oxygen at room temperature and forms a passive oxide film on its surface, that is composed of three layers: (1) TiO adjacent to metallic titanium, (2) TiO_x as an intermediate layer and (3) anatase TiO_2, which is in direct contact with the environment. On the other hand, oxidation at higher temperatures originate a crystalline oxide film, that is preferred in medical applications [Pouilleau et al., 1997]. To achieve the preferred passivation layer, a thermal oxidation of commercially pure titanium was performed under normal atmospheric conditions. (Skokan Edition 85 with a Bentrup TC 66 compact controller) While doing this, first unalloyed titanium wires with a diameter of 0.5 mm and a length[4] of 3 cm have been cleaned with acetone and ethanol in an ultrasonic bath for 25 minutes. Subsequently, the cleaned wires have been heated to 650°C at a heating speed of 5°C per minute. This temperature was hold for an hour and then the oven was switched off and the wires were cooled down to room temperature overnight. As stated by Gemelli et al., using these conditions leads to a preferred crystalline structure [Gemelli et al., 2007].

Scanning electron microscopy observations and cyclic voltammetry were carried out to evaluate the quality and structure of the oxide layer.

[4]The length of 3 cm has been chosen due to simple handling during assembly

3.2.2 Cyclic Voltammetry

The multichannel potentiostat (Bio Logic VMP3/P-01, France), that has been used for impedance spectroscopy measurements was also employed to confirm and evaluate complete sensor thermic passivation using cyclic voltammetry (CV) in the presence of an electroactive compound ferricyanide. Cyclic voltammetry measurements were carried out in a two terminal configuration consisting of a passivated titanium as working and an external platinum wire as the reference/counter electrode. A scan rate of 16 mV/s was chosen and the electric current was recorded in the absence and presence of 1 mM potassium hexacyanoferrate(II) trihydrate $K_4Fe(CN)_6 \cdot 3H_2O$ and 1 mM potassium hexacyanoferrite(III) $K_3Fe(CN)_6$ dissolved in phosphate buffered saline (PBS) [Villares et al., 2009; Sticker, 2015]. (Sigma-Aldrich, Germany)

3.2.3 Scanning Electron Microscopy (SEM)

SEM imaging was performed by colleagues at the Austrian Institute of Technology, Molecular Diagnostics in Vienna using a scanning electron microscope at 5 kV in high vacuum mode. (Zeiss, Supra40, Germany)

3.3 Inkjet Printing of Bendable Circuits on a Polydimethylsiloxane Surface

A normal resting heart beat for a healthy adult ranges between 60 to 100 beats per minute. This will result to an extraordinary mechanical stress on the sensor itself, that supposed to stay implanted in a cardiac tissue for several years. Particularly with regard to our research goal, a flexible sensor is crucial due to the curvilinear surface

and the mechanism and contraction events of a cardiac muscle. In order to achieve this flexibility, inkjet printed bendable circuits were tested to replace the conventional wiring of the implanted sensor in the long term.

3.3.1 Preparation PDMS Substrates

In order to fabricate a thin substrate, PDMS was mixed with a curing agent in the proportion of 10:1 by weight. (Sylgard 184, Dow Corning, USA) Air bubbles were removed by centrifugation at 400 rpm for 3 minutes. (Eppendorf, Germany) Degased PDMS was spin-coated on an acetone-cleaned, hydrophobic silicon wafer at 400 rpm for 30 seconds and precured at 75°C to achieve a substrate thickness of 250 µm [Sun et al., 2016]. (Laurell Tech. Corp., USA)

Polymerized PDMS substrate surface was then silanizated to achieve a sufficient bonding of inkjet printed circuits as published by Melnik et al. Therefore, a solution containing 5 % (v/v) (3-mercaptopropyl)trimethoxysilane (abcr GmbH, Germany) diluted with tetrahydrofuran (Sigma-Aldrich, Germany) and 0.4 % HCl (Sigma-Aldrich, Germany) was prepared. Subsequently, PDMS was activated in oxygen plasma and immersed in MPTMS solution for 1 hour. Then, PDMS was washed with isopropyl alcohol in ultrasonic bath for 5 minutes, two times in ultrapure water and once in 2-propanol. (Sigma-Aldrich, Germany) Subsequently, substrates were dryed in nitrogen steam [Melnik et al., 2014].

3.3.2 Inkjet Printing Silver Ink

The PDMS substrate was placed on a pre-heated Si-wafer and the total height was estimated as 750 µm in order to adjust the printer. Subsequently, the silver conductive

tracks (ANP Silverjet DGP 40LT-A, South-Korea) were patterned with a drop diameter of 70 µm on PDMS by a Dimatix inkjet printer (FujiFilm, 2831 series with a Cartridge DMS-11610, Japan) based on a CAD-designed layout as shown in Figure 3.3. After printing was finished, the PDMS substrates were heat treated by 150°C for 15 minutes.

3.3.3 Electrical Measurement

In order to evaluate the quality of the conductive tracks, two platinum conical probes were placed to contact the printed pattern and the resistance was measured by using a digital multimeter. (Isotech IDM67, Austria)

3.4 Oxygen Plasma Bonding of PDMS

Oxygen plasma bonding was used to bond top and bottom layer of the sensor together. A general protocol, that was also used during sensor fabrication is as follows. First, PDMS sheets were cleaned as shown in Section 3.3.1 and placed inside the chamber of plasma cleaner. The surface was then plasma activated at 700 mTorr chamber pressure for 30 s exposure time. (BlackHole-Lab, France) Subsequently, the activated PDMS surface can be bonded by pressing on another surface such as glass or another PDMS.

3.5 Electrode Configuration

There are several possible electrode configurations that can be used in order to measure tissue impedance. Within the scope of this thesis, a two-electrode or bipolar and a four-electrode, tetrapolar configuration were characterized and the influence of the electrode impedance on the signal response was evaluated. Therefor, a log-dilution

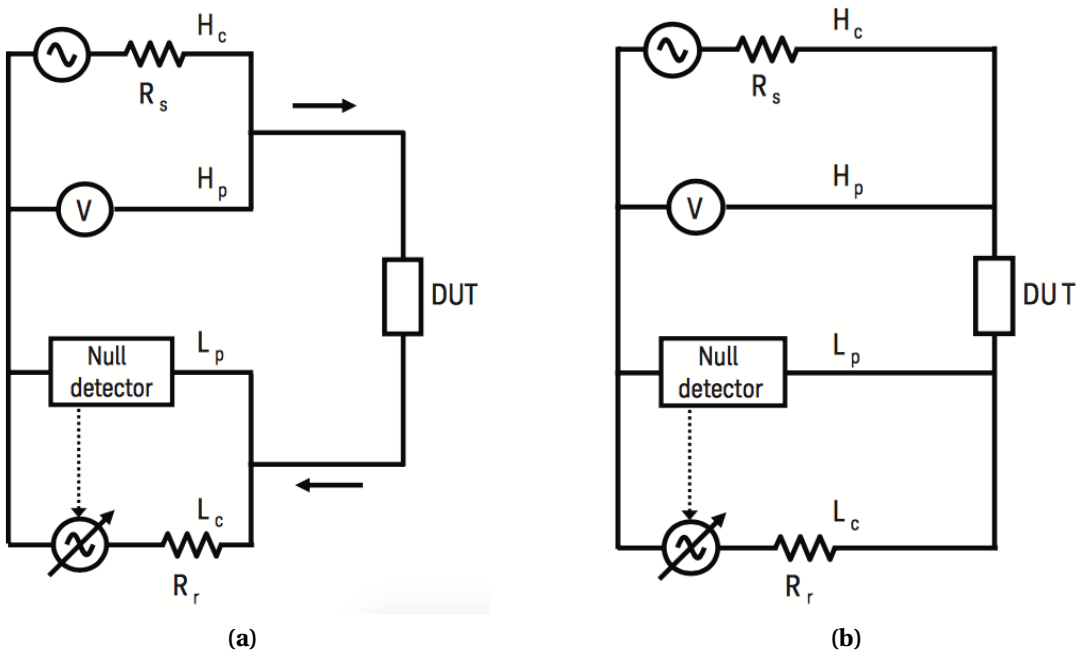

Figure 3.1: Schematic representation of electrode configurations used in electrical impedance measurements: **(a)** bipolar/two-electrode method and **(b)** tetrapolar/four-electrode method.

of NaCl solutions were prepared and a 100 mV peak-to-peak excitation voltage was applied in a frequency range from 10 Hz to 1 MHz to each of the solutions.

3.5.1 Two-Electrode Method

Performing electrical impedance measurement by applying the bipolar method means, that a known current is injected into the tissue under test through two electrodes (working and counter electrode) in order to measure the resulting drop of voltage between these two electrodes.

3.5.2 Four-Electrode Method

In contrast to the two-electrode method, in a tetrapolar setup a separate pair of electrodes (working and counter electrode) are being used to inject current in the

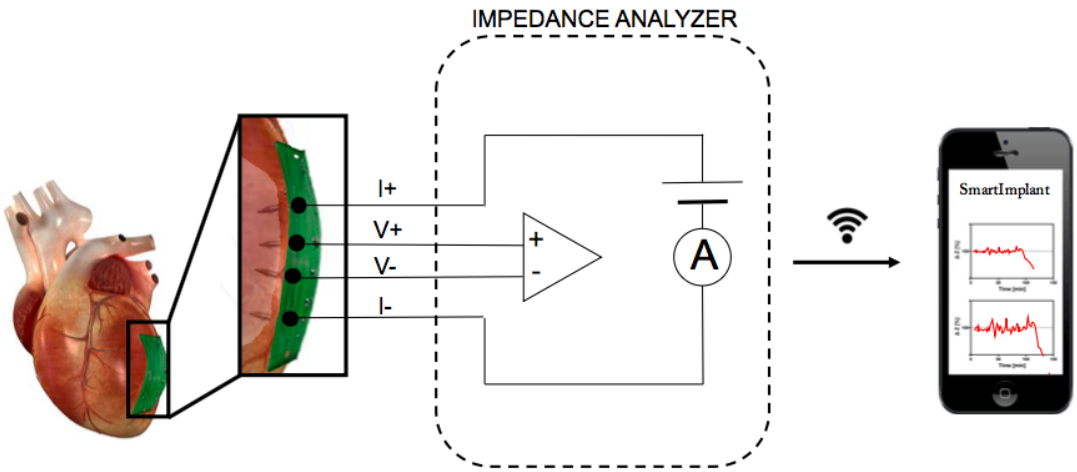

Figure 3.2: Sensor concept for cardiac rejection monitoring. The sensor will be surgically implemented at the time of transplant and allows a continuous monitoring with the use of state of the art wireless data transfer.

tissue and to measure the resulting voltage drop (working sense and reference electrode). In theory, since the current completely flows through the tissue and thus the electrode-tissue interface impedance has no influence on the sensor, a more accurate and precise impedance measurement is possible by eliminating direct discharges on the electrode surface.

3.6 Fabrication of Sensor Prototype

As shown in Figure 3.3 a sensor layout[5] for a tetrapolar electrode setup containing a top and bottom layer was designed by using AutoCAD to meet the specific geometrical requirements of a rabbit heart[6] as shown in Table 3.1 [Noszczyk-Nowak, 2009]. Figure 3.5 illustrates the assembly procedure. The layers were cutted by a CNC laser cutter. (Universal Laser Systems, USA) To establish a connection between electrodes and

[5] Bi- and tetrapolar measurements are possible by varied electrode contacting of inner and outer electrodes, however the results cannnot be quantitatively due to a different geometrical constant based on a different electrode distance.

[6] Rabbit heart might be used in further pre clinical development stages.

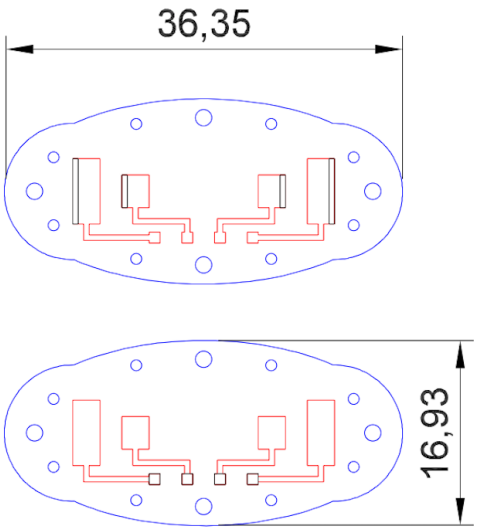

Figure 3.3: CAD sensor design with top and bottom layer for CNC cutter and inkjet printing. (blue: lines were the PDMS was cutted, black: electrodes and red: layout for inkjet printing)

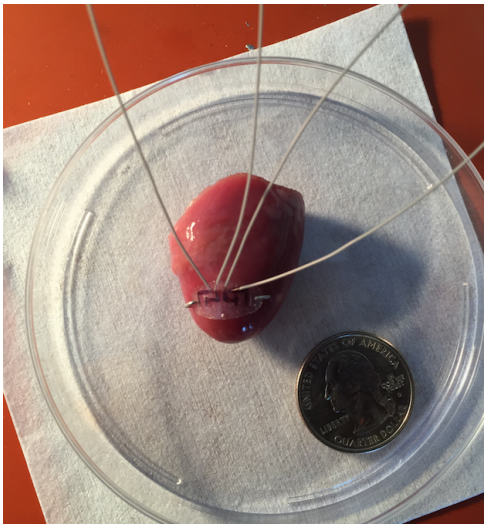

Figure 3.4: Illustrative presentation of the PDMS sensor placed on a chicken heart sample

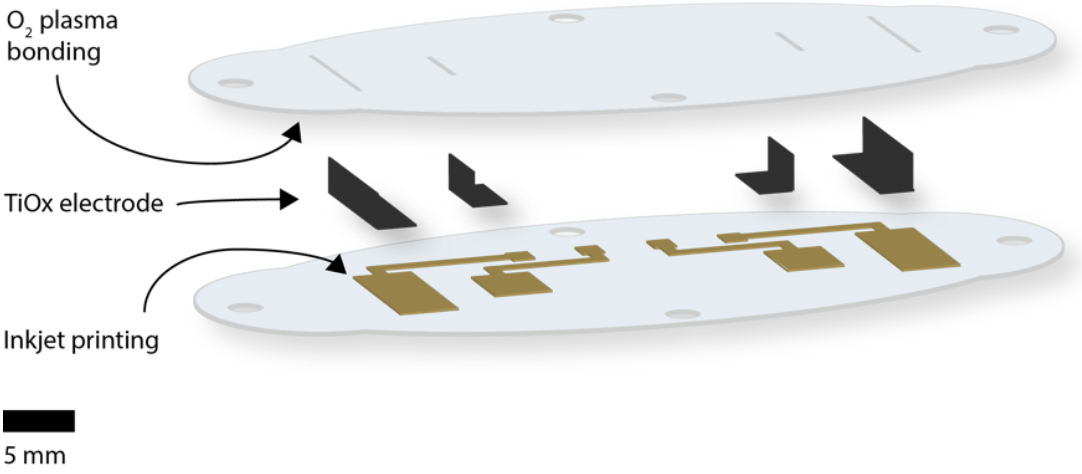

Figure 3.5: Fabrication flow of two-layer microdevice containing passivated titanium dioxide electrodes. Conductive tracks were inkjet printed on one sealing the electrodes with another PDMS layer using plasma bonding.

Table 3.1: Macroscopic dimensions of the heart of European brown hares [Noszczyk-Nowak, 2009].

Parameter	Mean value and SD
Length of the heart (mm)	53.33 ± 9.0
Width of the heart (mm)	39.00 ± 2.82
Myocardial thickness (mm)	8.66 ± 1.5

measurement electronics, on the bottom of the top layer, inkjet printed conductive tracks guide the measurement signal to an external potentiostat as discussed in Section 3.3. Passivated titanium dioxide electrodes were fabricated as shown in Section 3.2 and bended so that a maximum length of 3 mm for inner and outer electrodes and a width of 3 mm for inner and 6 mm for outer respectively were achieved. The distance between the two inner electrodes is 10 mm and between the outer and inner electrode 5 mm. The passivation layer on one end of the electrode was rubbed off by using a commercial scratch paper. The electrodes were then fixed with the scratched end on the inkjet printed tracks with a conductive silver paste and dried for 2 h at 75°C. (Sigma-Aldrich, Germany) Subsequently, oxygen plasma was used to bond top and bottom part together in order to seal the sensor hermetically as shown in Section 3.4.

3.7 Characterization of Sensor

3.7.1 Electrical Testing of Measurement Setup

The experimental setup was evaluated by measuring four reference resistors (10, 100, 1000 and 10.000 Ohm) at the same 30 frequencies between 10 Hz and 1 MHz in a galvanostatic mode by applying a 10 mA alternating current such that the effects of instrumentation can be observed. In general, in order to avoid pick up effects no

measurements were made at 50 Hz. A pure resistor exhibits no phase shift between the voltage and current, thus the measured impedance consists exclusively of a real component and thus according to (2.10).

$$Z_{Resistor} = R \tag{3.1}$$

In order to bring these effect even more into focus, the percentage error between measured and theoretical value was calculated according to (3.2).

$$\%_{ERROR} = \left| \frac{\#_{measured} - \#_{theoretical}}{\#_{theoretical}} \right| \times 100 \tag{3.2}$$

3.7.2 Determination of Geometric Cell Constant

The cell constant κ is the scaling constant between the specific conductivity σ of the medium against the conductance measured by the sensor, as shown in equation (2.16). Gabriel et al. stated that, although there are theoretical methods available to estimate, it is much easier and more accurate[7] to determine the cell constant experimentally [Gabriel et al., 2009]. In aquaous NaCl, a linear relationship between conductance and concentration can be assumed as shown in (2.14) Therefor, a dilution series of NaCl was prepared ranging from 0.001 to 0.15 M and analyzed impedametrically at eight frequencies in the range of 10 Hz to 300 kHz[8] by applying an alternating current with an amplitude of 10 mA at room temperature. (Sigma-Aldrich, Germany) Since theoretically, there is no dielectric dispersion at frequencies below 500 kHz in an aqueous NaCl solution, experimental impedance data can be used to determine the electrical

[7] In order to calculate the cell constant theoretically, an exact information of the electrode surface area and electrode distance is necessary. Especially in case of a passivated electrode, is the determination of the surface area fraught with problems.

[8] The frequency range has been choosen based on previous measurements in Section 3.5.1

conductivity by plotting the obtained conductance values against conductivity values published by Peyman et al. [Peyman et al., 2007]. The cell constant is then obtained by the slope of the regression line.

3.7.3 Determination of Sensor Sensitivity

The identical setup of Section 3.7.2 was used in order to quantificate the sensitivity of the sensor with regard to the ionic strength of a solution. We define the sensitivity as the slope of the regression line of the concentration and the associated impedance on a logarithmic scale as shown in (3.3)

$$\log Z = Z_0 + \lambda \times \log c \tag{3.3}$$

where λ is the sensitivity, Z is the measured electrical impedance, c is the salt concentration and Z_0 is the impedance for c→0. At low concentration also Z_0→0 and thus, λ can be expresssed as

$$\lambda \approx \frac{\Delta \log Z}{\Delta \log c} \tag{3.4}$$

Needles to say, that changes in ionic strength of a medium aren't the only reason for changes in electrical impedance, however λ is a good value in order to meet a first approximation of the sensor's sensitivity.

3.7.4 Impact of Temperature Changes on Electrical Impedance

The effect of temperature changes on the measured impedance has been discussed in Section 2.2.3 already. In order to quantificate this impact, measurements of the electrical impedance were carried out at physiological relevant body temperatures

from 26 to 44°C in 100 mL 1x PBS at 100 kHz by applying an alternating current with an amplitude of 10 mA. A magnetic stirrer was used in order to distribute heat evenly.

3.8 Cell Culture

Jurkat cell line (ATCC®, TIB-152™) were cultured in an advanced RPMI 1640 media (BioWhittaker®, BE12-702F) with L-glutamine supplemented with 10 % heat-inactivated fetal calf serum and 1% antibiotic-antimycotic solution (Biowest, L0010). For routine growth, the cells were maintained in an incubator at 37°C with a 5 % CO_2 humidified atmosphere. Cells were split with fresh media when the culture reached confluency and a change in color due tue a pH indicator could been detected, respectively.

3.9 Impedance Spectroscopy

A commercial multichannel potentiostats (Bio Logic, VMP3/P-01, France) was employed for impedance spectroscopy measurement controlled by the EC-Lab V11.02 software enabling parallel measurement of currents down to 1 nA in the frequency range between 0.1 mHz and 1 MHz. Since part of the research activities were carried out at the Bioengineering Department at University of California, another precision LCR meter had to be used for measurements on site (Keysight, E4980A, USA). However since there was no commercial software available, a Python program needed to be written in order to send SCPI commands to the LCR meter and measure electrical impedance over a logarithmic frequency sweep. A complete Python command can be found in Appendix.

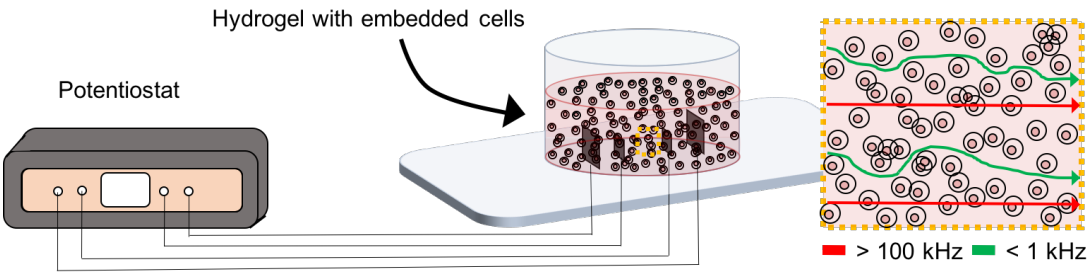

Figure 3.6: Graphical description of immune cell infiltration. Jurkat cells were embedded in a hydrogel in order to simulate the influx of immune cells in a rejected tissue

3.9.1 Sample Preparation for in vitro Impedance Spectroscopy of Mammalian Cells

Once the cell culture reached confluency, Jurkat cells were concentrated to achieve a higher cell concentration. Therefor, the cell suspension was centrifugated at 400 rcf and a part of the supernatant was discarded and used for blank measurements. Cell number was determined by counting manually using a hemacytometer. As depicted in Figure 3.6 cells were then mixed with a previously prepared low gelling agarose at 37°C in order to achieve a final concentration of 10^7, 10^6, 10^5, 10^4 and 10^3 cells per mL, transferred to a Transwell plate and hardened at 10°C. (SigmaAldrich, Germany) A hydrogel without cells using the same amount of cell culture media was also prepared for a blank measurement.

3.9.2 Preparation of Low Gelling Agarose

200 mL RPMI 1640 media and a stir bar were added to a beaker and 2 g agarose powder was sprinkled into the liquid while stirring in order to prevent clumping. Beaker and solution was weighted in order to determine volume changes due to heating. Subsequently, the solution was boiled for 5-10 min stirring continuously until agarose was dissolved completely. Hot distilled water was added to return the original

weight and correct for evaporation. Gel was then stored at 10°C.

3.9.3 Organ Sample Preparation for ex vivo Impedance Spectroscopy in Tissue

In order to obtain a more accurate tissue environment that is similar to a rejected cardiac implant of a patient, animal tissue samples were examined. To evaluate how structural changes in tissue ex vivo correlate with the simulation and directly influences the dielectric properties, in the next set of experiments a tissue degradation model has been analysed for commercially available chicken hearts. For the purpose to simulate pathological changes in tissue, two different experiments were planned and carried out. Therefor, the sensor was implemented in the sample, that was then placed in a physiological saline bath allowing continuous monitoring of structural changes withing the tissue and alteration of electrical impedance during experiments. On one hand, heart tissue has been freeze-thawed up and compared with the electrical impedance spectra of fresh and untreated samples. To compare physical with biochemical degradation processes, in the next set of experiments whole chicken heart samples were subjected to enzymatic digestion for 24 hours using a sterile trypsin/EDTA containing sodium chloride solution as depicted in Figure 3.7, at 37°C in order to simulate a degradation of tissue. (Sigma-Aldrich, Germany) It was considered to avoid evaporation the solution and thus a decrease of volume, that would lead to an artificially higher impedance. Chronic organ rejection is a complex process that takes place over several days and weeks of hospitalization [Kittleson et al., 2017]. Therefore, enzymatic tissue decomposition following the same protocol as described for single measurements was also monitored in a time-resolved manner to mimic tissue degradation during rejection over time.

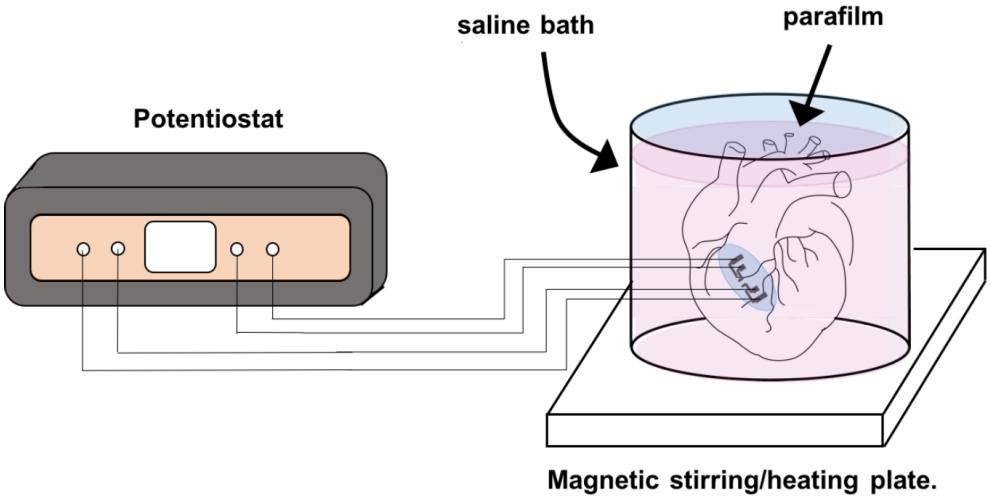

Figure 3.7: Experimental setup for trypsinization of heart tissue. Degradation of chicken heart tissue samples were monitored over a frequency range between 10 Hz and 500 kHz fpr 24 h at 37°C.

3.9.4 In vivo Myocardial Impedance Analysis

Ex vivo tissue impedance analysis is a useful technique to analyse biological status of a tissue qualitatively. Additionally, with regard to a continuous rejection monitoring and using an implanted device, in vivo analysis of myocardial impedance was measured in a 35 kg female juvenile Yucatán mini pig. Access to the heart was done via median sternotomy under a general endotracheal anesthesia and the impedance sensor was placed on the apex of the left ventricle with the electrodes being inside the myocardial tissue as shown in Figure 3.8[9]. On one hand, a logarithmic frequency sweep was performed in the frequency range between 100 Hz and 1 MHz using a 100 mV sinusoidal signal in a potentiostatic mode. On the other hand, at a choosen frequency of 5 kHz, myocardial impedance of a beating heart was recorded with a sampling rate of 150 ms[10].

[9] Open heart surgery was performed by Prof. Wieselthaler and Jarrett Moyer at the University of California, San Francisco. Myocardial impedance was recorded with a Keysight E4980A LCZ meter. Custom made Python code can be found in Appendix.

[10] Limit of detection with the equipment used.

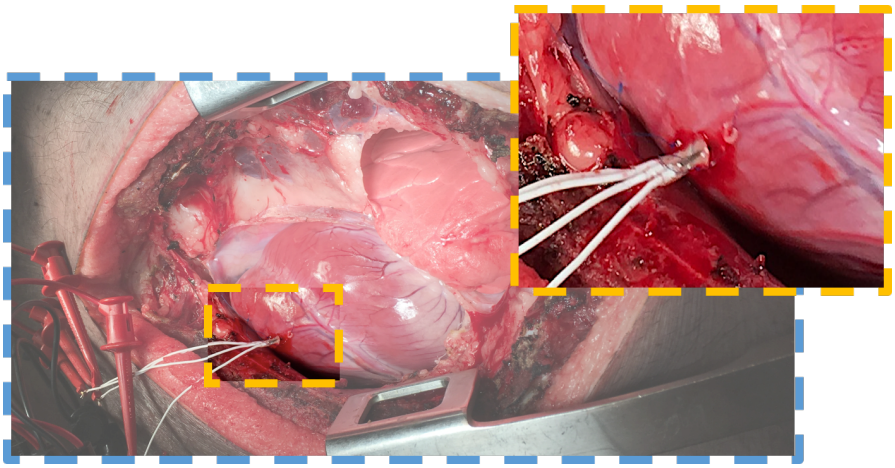

Figure 3.8: Surgical setup for in vivo myocardial impedance analysis in a beating heart. Open heart surgery and sensor implantation were performed on a Yucatan mini pig at University of San Francisco, California.

3.10 Computer Modeling of Tissue Impedance

Developed by Ivorra et al., a circuit analysis software package (SPICE OPUS 2.03) was used to validate, if bioimpedance sensing is particularly sensitive towards cell morphology changes and tissue remodeling events during the process of rejection by simulating the electrical impedance of living tissue [Ivorra, 2005]. To achieve

Table 3.2: Electrical and physical constants used during SPICE simulation

Constant	Value
Slab thickness	50 µm
Pixel size	5 µm * 5 µm
Number of pixels	200 × 200
Electrode resistivity	0 Ω cm
Intracellular resistivity	100 Ω cm
Extracellular resistivity	100 Ω cm
Membrane capacitance	1 µF/cm^2
Membrane resistance	1 GΩcm^2

this objective, a two-dimensional image of a tissue has been sketched based on a histological examination [Noszczyk-Nowak, 2009] and converted into its equivalent

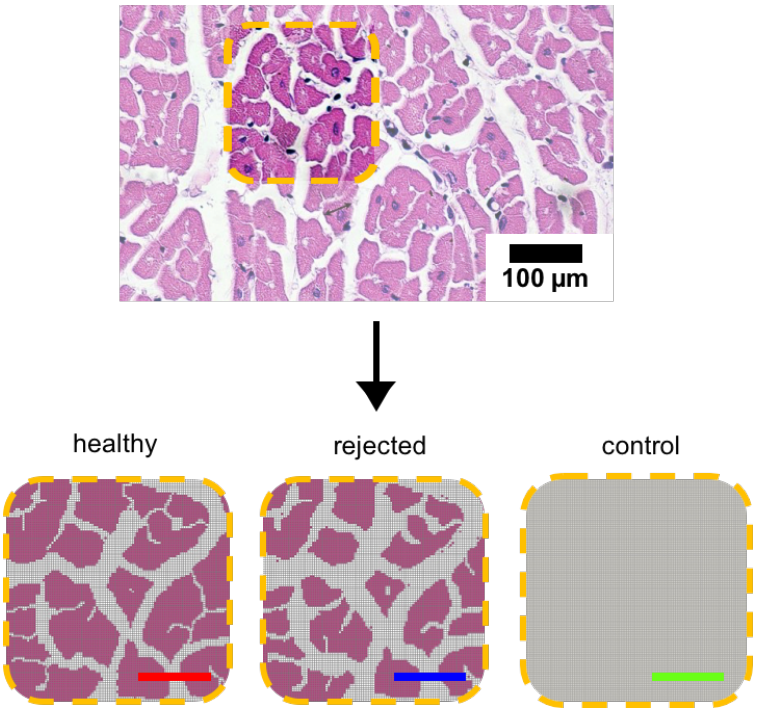

Figure 3.9: Graphical description of the simulation model of tissue rejection based on a histologicalcross-section examination of a rabbit cardiac tissue [Noszczyk-Nowak, 2009].

circuit elements as a model of extracellular space expansion, which is beside the infiltration of immune cells, one of the key histopathological symptoms during cardiac rejections [Costello et al., 2013]. The simulation performs a frequency sweep from 10 Hz to 1 MHz, which is comparable with the experimental settings. Artifacts such as capacitive leakage at higher frequencies and polarization effects at frequencies below 1 kHz cannot be simulated by this approach.

3.11 Correction of Experimental Data

Polarization effects and interferences at low frequencies that may occur at the surface of the electrodes and therefor influence the impedance measurement accuracy can been avoided by using passivated electrodes in a tetrapolar setup as shown in Figure 4.4. However, at higher frequencies above 100 kHz, the presence of stray capacitances

creates a measurement artefact that has been discussed by Buendia et al.. To minimize these effects, measurement values were corrected by estimating the parasitic capacitance from the suspectance of the measurement [Buendia et al., 2010].

4 Results and Discussions

4.1 Sensor Characterization

4.1.1 Electrical Testing of Measurement Setup

Figure 4.1a shows the results of the electrical testing. There is just a slightly variation in the measured resistance as a function of frequency and shows constant values for low and middle frequencies. However, in the region above 100 kHz the effects from stray capacitances are at a maximum, which results in an artifically increased resistance value. The corresponding resistance spectra present an even less coherent picture, if the resistor is 1 kOhm or higher. This becomes even more evident by looking on the positive percentage error between measured and exact resistance value as shown in Figure 4.1b. Based on the literature, there is no impedance value above 1 kOhm to be expected in a biological tissue, however systematic measurement errors like these need to be considered and corrected, as the circumstance requires.

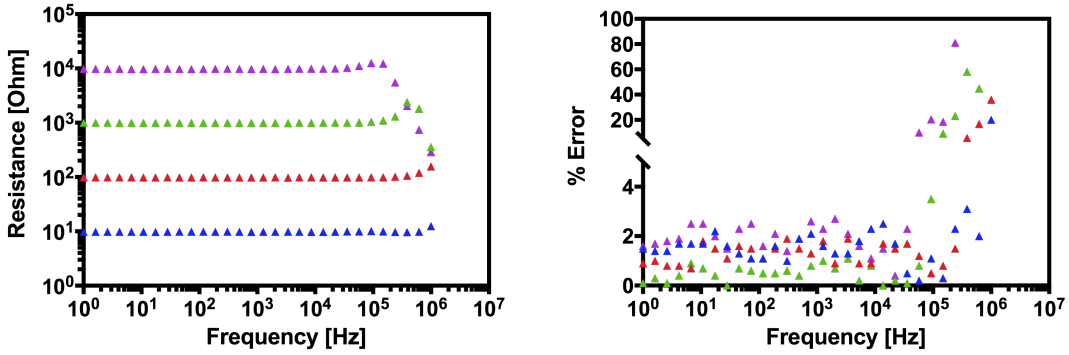

(a) (b)

Figure 4.1: Evaluation of systematic errors by measuring four commercial available reference resistors (blue: 10 Ohm, red: 100 Ohm, green: 1 kOhm and purple: 10 kOhm) **(a)** Measured resistance **(b)** the percentage error between measured and exact resistance value.

4.1.2 Electrode Passivation

Results of Scanning Electron Microscopy

To evaluate the quality of the oxidation layer on the electrode surface, scanning electron microscopy was performed on thin sections. An insulating layer of titanium dioxide can be observed on the planar surface of the titanium electrode. The passivation layer thickness is not laterally homogenous and varies from 400 to 800 nm as can be seen in Figure 4.2, however together with the voltammetry results it can be concluded, that the passivation process was sucessful, the total electrode surface is covered and the electrodes can considered to be electrically isolated.

Results of Cyclic Voltammetry

In order to further evaluate the homogenity of the formed titanium dioxide electrode interface, cyclic voltammetry is performed for pristine and thermally oxidated titanium dioxode electrode in a 1 mM ferricyanide solution. Figure 4.3 displays a scan at a clean titanium electrode recorded in 1 mM ferricyanide solution, overlaid with a scan

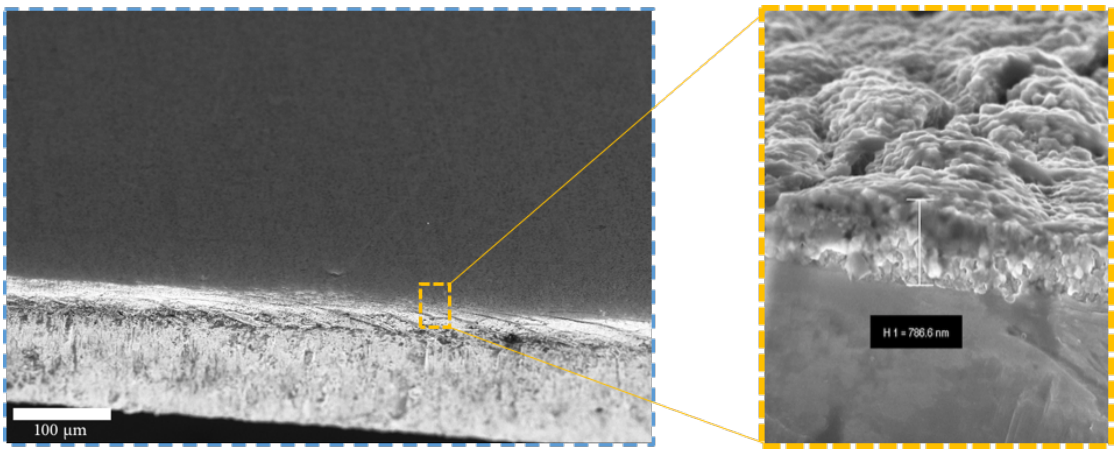

Figure 4.2: Scanning electron microscopy (SEM) images of electrode surface at different solutions. SEM imaging was performed at 5 kV in high vacuum mode. (Zeiss, Supra40)

for a thermal oxidated electrode with an appr. 500 nm titanium dioxide passivation layer in the same solution. For pristine titanium electrodes with thin and inhomogeneous titanium dioxide layers, that naturally form due to atmospheric oxidation [Feng et al., 2002] a characteristic voltammogram with a peak current of 350 mA was detected. In contrast, thermal oxidation results in a homogenous and complete covered titanium dioxide interface that results in severe decrease in non-faradaic charge and current flow on the electrode surface. Titanium dioxide is frequently applied and well characterized for application in tissue engineering and implantology [Ratner et al., 2008; Balazic et al., 2007]. Therefore, thermal oxidation under atmospheric conditions is an effective and straight-forward method to increase biocompatibility of titanium surfaces [Wang et al., 2016] in contrast to other physical and chemical surface modification strategies [Kwasniak et al., 2015]. All in all, a succesful sensor insulation by thermal oxidation and thus an decrease of charge transfer was confirmed using an electroanalytical technique.

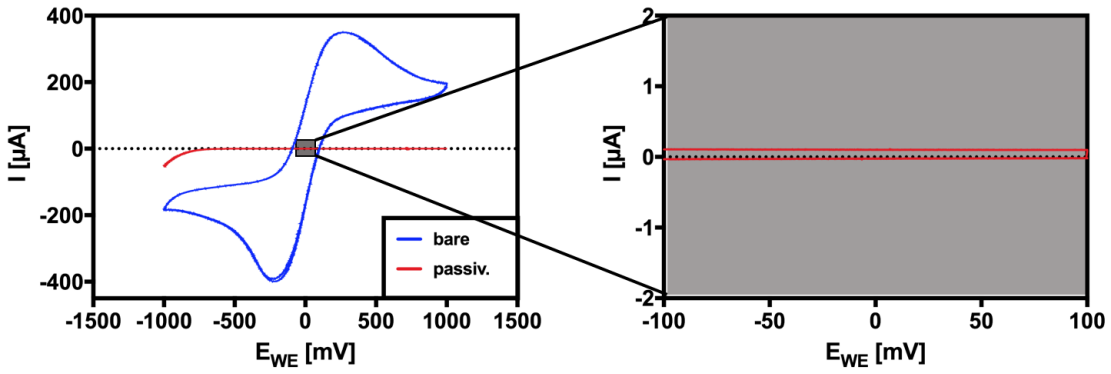

Figure 4.3: Overlaid cyclic voltammograms for a bare titanium electrode and a thermal oxidated titanium dioxide electrode. Recorded in a ferricyanide solution at 50 mV/s. Blue curve shows untreated titanium electrodes and red curve shows thermally passivated electrodes with appr. 500 nm titanium dioxide layer.

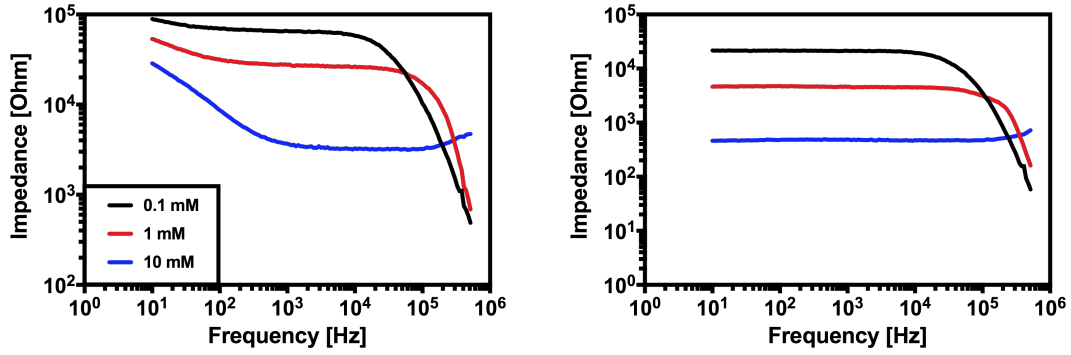

Figure 4.4: Measured electrical impedance Z [Ohm] with bi- and tetrapolar electrode setup. NaCl solution with a concentration of 0.1 (black), 1 (red) and 10 mM (blue) was used.

4.1.3 Comparison of Two and Four Electrode Configuration

Electrical impedance spectre of 1 mM NaCl in a two and four electrode setup were compared by using the same electrical parameters. The resulting spectra can be divided into three characteristic frequency bands: (1) below 1kHz, (2) 1-100 kHz and (3) above 100 kHz. Theoretically, ionic solutions such as aqueous NaCl exhibit no dielectric dispersion at frequencies below 1 MHz [Gabriel et al., 2009]. By using a bipolar setup however, an additional impedance can be observed below 1 kHz, that is

mainly due to an occuring electrical-double layer at the electrode/electrolyte interface and decreases with increasing frequency. At the first glance it can be also observed, that the overall magnitude of the exact same solution differs significantly between the bi- and tetrapolar configurations, however the absolute values of the impedance modulus are not comparable since they do not rely on the same geometric cell factor. Decreasing impedance above 500 kHz was found appropriate to consider as a general measurement error due to capacitive leakage.

Thus, it can be stated, that the influence of the electrode impedance on the response can be minimized by using a tetrapolar electrode setup. An even wider linear range up to 100 kHz can be achieved at physiological concentrations, that is of particular importance, when it comes to engineering medical devices.

4.1.4 Determination of Geometric Cell Constant

Admittance, the inverse of the electrical impedance, was used to extract the measured conductance values. As stated in Section 3.5.2, there is no dielectrical dispersion and thus no imaginary part below 500 kHz in an aquaous saline solution. Therefor, the measured admittance consists exclusively of a real component; thus, it can be equated to conductance. Based on the results of Section 4.2, frequencies below 300 kHz were used in order to eliminate any possible system error. As expected, it can be seen from Figure 4.5a, that the measured conductance doesn't vary within the chosen frequency range. Fairly variation due to experimental artifacts, temperature changes between samples and electrode polarization at lower frequencies can still not be excluded entirely. However, in general the standard deviation stays below an acceptable three percent. At a physiological concentration of 0.15 M, which is of particular interest in medical research, an even lower standard deviaton of 0.76 percent was calculated.

Table 4.1: Determination of cell constant: average conductance (G) [Siemens] of aquaous saline solutions from 100 Hz to 300 kHz; the conductivity (σ) [Siemens/m]

NaCl [M]	G [S]	G [S] SD	G [S] SD	σ [S/m]
0.001	2.21E-04	4.92E-06	2.23 %	0.009
0.005	6.65E-04	1.04E-05	1.57 %	0.047
0.01	9.75E-04	2.96E-05	3.04 %	0.094
0.03	3.06E-03	3.10E-05	1.01 %	0.281
0.05	4.83E-03	2.95E-05	0.61 %	0.466
0.15	1.12E-02	8.45E-05	0.76 %	1.375

* Conductivity values were taken from Peyman et al. Peyman et al. [2007]

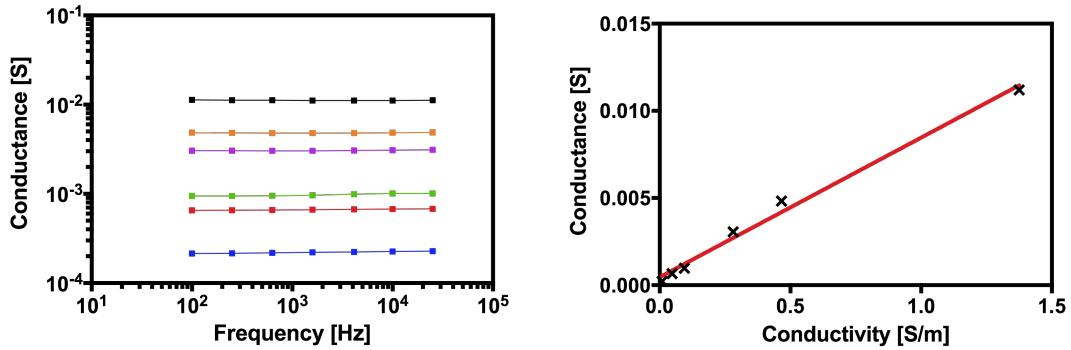

(a) (b)

Figure 4.5: Determination of geometric cell constant: **(a)** frequency independent conductance by using a tetrapolar setup below 300 kHz (black: 0.15 M, orange: 0.05 M, purple: 0.03 M, green: 0.01 M, red: 0.005 M and blue: 0.001 M NaCl) **(b)** linear regression between measured conductance and conductivitiy values of NaCl solutions, which have been used to calculate the cell constant. (y=0.008x + 0.0005; R^2=0.99) [Peyman et al., 2007].

Exact values can be found in Table 4.1. On the other hand, there is a strong correlation; thus, a linear relationship between conductivity and conductance with an R^2=0.99 as shown in Figure 4.5b. The geometric cell constant of the sensor was found to be 0.008 m.

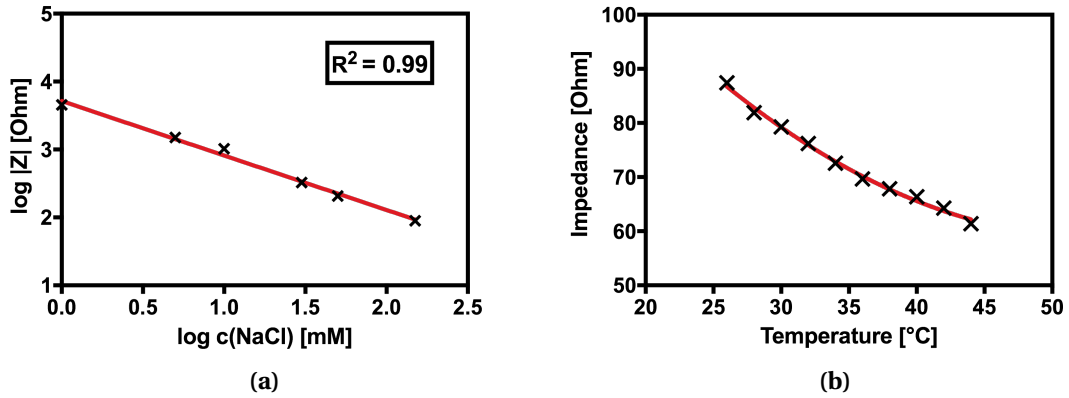

Figure 4.6: Characterization of sensor. **(a)** Determination of sensor sensitivity: concentration series of aquaous NaCl at significant frequencies results in a linear regression between measured electrical impedance and NaCl concentrations. (y=-0.8021x + 3.714, R^2=0.99) and **(b)** the impact of temperature changes on electrical impedance of a 1X PBS at 100 kHz. Best fitting achieved with a second order polynomal correlation (R^2=0.99)

4.1.5 Determination of Sensor Sensitivity

In Section 4.2.4 the dependence of the measured conductance and thus the electrical impedance on the electrolyte concentration was proven. The same dataset was also used in order to determine the sensitivity of the sensor as defined in equation (3.3). In Figure 4.6a, concentration series of aquaous NaCl were plotted against measured impedance values on a logarithmic scale. Since the measured impedance doesn't vary within the chosen frequency range at low ionic strength either, a mean of the measured impedance values was used calculating the sensor sensitivity. Therefor, according to equation (3.4), the sensitivity was calculated to be λ=0.8, which means that for a Δc of 1 mM a ΔZ of 6,3 $\times$ Δc can be measured. This can be considered as significant compared to the standard deviaton of approx. 2 % at a physiological concentration of 150 mM NaCl.

4.1.6 Impact of Temperature Changes on Electrical Impedance

To understand, how changes in tissue temperature during organ rejection due to post-transplant fever [Fishman, 2007] have an impact on the rejection monitoring device, impedance spectroscopy is performed under physiologically relevant temperature regions using phosphate buffered saline solution. Figure 4.6b shows changes in impedance with varying temperature within a physiological relevant range. The measured impedance decreases with increasing temperature to a second polynomal degree. In summary, due to a decrease in viscosity at higher temperatures, the resistance; thus, electrical impedance decreases due to an increasing ionic mobility as shown in equation (2.12). This changes are negligible compared to impedance changes due to an alternating ionic strength. However, since tissue rejection is especially hallmarked by the process of inflammation; thus, an increase of body temperature locally and in general, a consideration of additional measurements of the body temperature might be an interesting feature with regard to the future of sensor development. In order to avoid any influence of temperature on the following experiments, temperature was held constant at all times.

4.2 Inkjet Printing of Bendable Circuits on a Polydimethyl-siloxane Surface

In order to achieve a flexible sensor design, an inkjet printing process of bendable circuits on PDMS was tested. First, "homemade" PDMS sheets were sucessfully prepared and treated as described in Section 3.3.1. Unfortunately, there had to be dealt with some unforeseen complications during the actual printing process. On one hand, a great deal of so-called comets, which are droplets of ink on PDMS, where

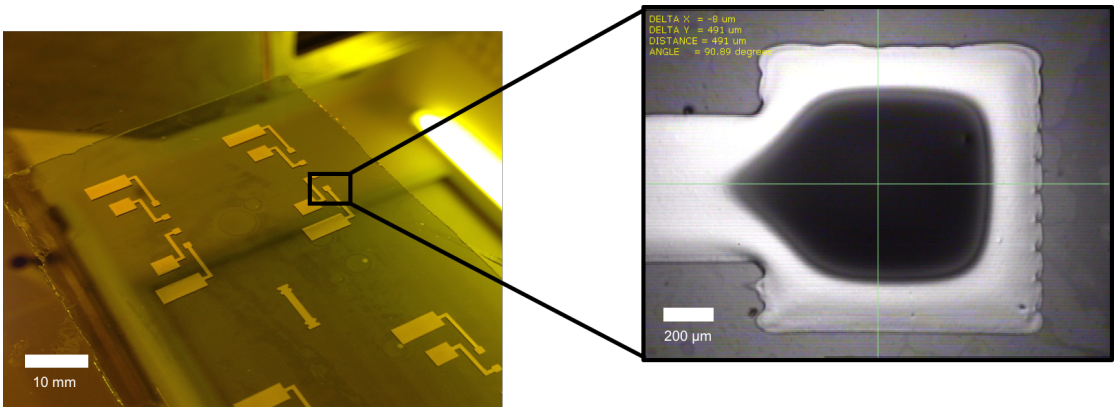

Figure 4.7: Succesful inkjet printing of conducting silver ink on a PDMS sheet with a sheet resistance of 83 Ohm per square.

no structure should be printed, occured. Especially, on areas with larger structures has this phenomenon been observed. Small structures such as contact pads and conductive tracks have clear printing lines as can be shown in Figure 4.7. On the other hand, cracks within the printed structures were visible, after removing PDMS sheets from the wafer, that can lead to a non-conducting structure. In order to avoid that, it was suggested to place the PDMS sheet on a polymer foil. All things considered, the printing process was succesful and a resistance of 80 to 90 Ohm per sqare was measured, depending on the applied pressure on the conical probes of the digital multimeter on the printed circuits.

4.3 Results of Multi-frequency Tissue Impedance Simulation

Prior impedimetric analysis of biological tissue samples, computer simulations have been performed to evaluate the influence of cellular and acellular components, such as integrity and morphology on electrical impedance in biological tissue. As shown in Figure 4.8, changes in tissue integrity are visible at characteristic frequencies between

100 Hz to 100 kHz in imaginary and real part of the electrical impedance spectra. As shown in Figure 4.8a, at a frequency range above 1 kHz characteristic β dispersion can only occur in tissue and is not detectable for saline solutions [Grimnes and Martinsen, 2015]. Additionally, significant decrease of resistance due to changes in tissue integrity and an alteration of extracellular space, current will pass more easily across the tissue, leading to a reduction in the resistive part of the impedance in comparison to physiological and intact tissue structure. Figure 4.8b shows a significant decrease of reactance at approx. 1 kHz due to simulated disruption of cell integrity and an alteration of cell membran capacitance compared to viable tissue. Altough the resistive part that is directly proportional to the resistance and therefor to the ion composition of biological fluids, in acellular controls no reactance was detectable due to lack of cell membranes.

As has already been explained in Chapter 2.1, during an onset of rejection, immune cells infiltrate the implanted graft causing devastating damage to its morphological integrity. Based on these simulations, it can be expected, that these changes in the electrophysiological properties of cardiac implants lead to an alteration of the electrical resistance and reactance within the β dispersion range.

4.4 Mathematical Correction of Tissue Impedance Results

In order to minimize effects of stray capacitances, measurement values were corrected by estimating the parasitic capacitance from the suspectance of the measurement. Buendia et al. defines a complex function for correction of measured data as shown in (4.1),

$$Z_{corr}(\omega) = Z_{meas}(\omega)\frac{1}{1 - j\omega Z_{meas}(\omega)C_{par}} \tag{4.1}$$

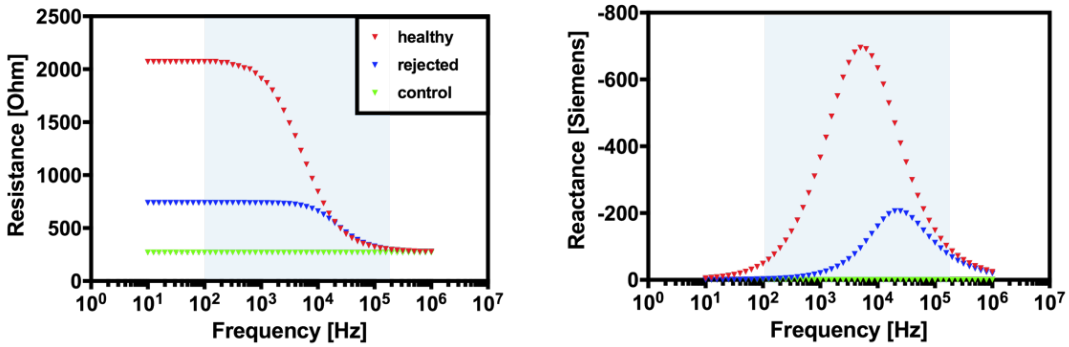

Figure 4.8: Computer simulation of a tissue rejection process: **(a)** Real and **(b)** imaginary part of simulated electrical impedance for healthy and rejected tissue. Changes in tissue integrity are visible at characteristic frequencies in imaginary and real impedance spectrum.

where Z_{corr} and Z_{meas} are the measured and corrected impedance respectively, ω is the frequency in the unit of radian and C_{par} the parasitic capacitance, that is estimated by the slope of the regression between frequency and suspectance as shown in Figure 4.9a. According to equation (2.10)

$$Z_{corr}(\omega) = R_{corr} + jX_{corr} = \frac{R}{N} + \frac{j(\omega R^2 C_{par} + X + \omega X^2 C_{par})}{N} N \tag{4.2}$$

where N is defined as

$$N = 1 + 2\omega X C_{par} + 2(\omega X C_{par})^2 \tag{4.3}$$

Mathematical relations lead to equation (4.4) and (4.5) which solutions R_{corr} and X_{corr} are nothing else but the corrected resistance and reactance.

$$R_{corr} = \frac{R}{N} \tag{4.4}$$

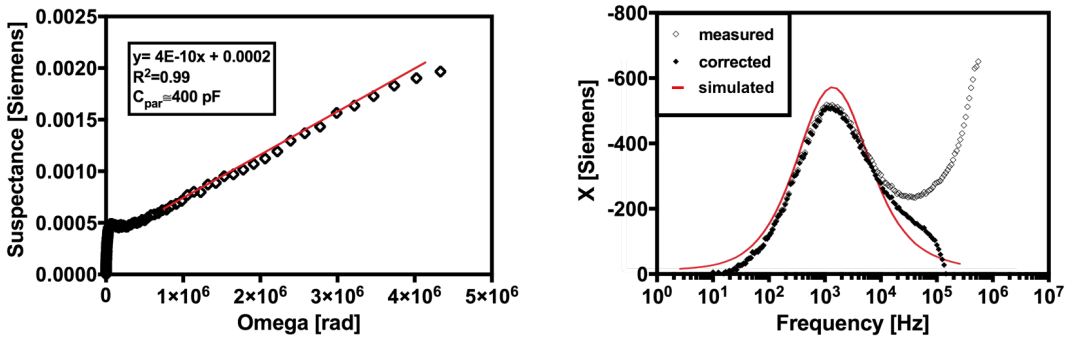

(a) **(b)**

Figure 4.9: Removing the capacitive leakage artifact from electrical bioimpedance measurements in tissue **(a)** stray capacitance has been estimated to be appr. 400 pF and **(b)** shows the result of correction function.

$$X = \frac{\omega R^2 C_{par} + X + \omega X^2 C_{par}}{N} \tag{4.5}$$

This correction function is valid up to 600 kHz and therefor it should work fine with our measurement setup. As shown in Figure 4.9b, the correction function does not alter the reactance values below 10 kHz, where parasitic capacitance is negligible, however at higher frequencies, measured reactance values could been succesfully corrected, so that after correction, simulated and measured values converge very well with each other.

4.5 Experimental Results of Impedance Spectroscopy

4.5.1 In vitro Impedance Spectroscopy of Mammalian Cells

As depicted in Figure 3.6, in order to establish a model to simulate the influx of immune cells into a cardiac tissue, various concentration of Jurkat cells were embedded

in a hydrogel and the impedance was measured using a 5 mA peak amplitude at frequencies logarithmically spaced in the range of 10 Hz to 500 kHz. In this experiment, hydrogel should replace the extracellular scaffold and simulate the structure and integrity within a biological tissue, while the embedded cells simulate the influx of immune cells during a rejection process. Figure 4.10a shows the measured impedance averaged over the sweeped frequency range. Compared to a blank hydrogel, that has an impedance of 57.22 ± 0.78 Ohm, for a cell concentration of 10^7 cells per mL an impedance of 136.92 ± 3.08 Ohm was measured. At first sight, there also seems to be a direct correlation between the impedance signal of the embedded Jurkat cells with a limit of detection at about 10^5 cells per mL. However, as shown in Figure 4.10b and 4.10c, there is no dispersion in the resistance signal and there is almost no reactance. Based on the theory and the simulation results as shown in Figure 4.8, in the presence of an AC electrical field, distinct relaxation modes occur in multicellular system, mainly due to interfacial polarization along membranes and ion fluctuations within biofluids, that lead to a reactance signal within the kHz range. In this case, the impedance signal is only influenced by the resistive properties of the hydrogel. At high cell concentration between 10^7 and 10^5 cells per mL, higher resistance may be caused just by volumetric changes of hydrogel due to a higher concentration in cells, which again leads to a high impedance signal. Unfortunately, this model cannot be used for the simulation of tissue infiltration by immune cells.

4.5.2 Ex vivo Simulation of Tissue Degradation

To mimic changes in morphological tissue integrity experimentally, organ samples were subjected to a freezing-thawing cycle to disrupt cell membranes. As seen in Figure 4.11, the ex vivo impedance analysis correlates very well with the previous simulation data shown in 4.8. On the one hand, Figure 4.11a shows that physical

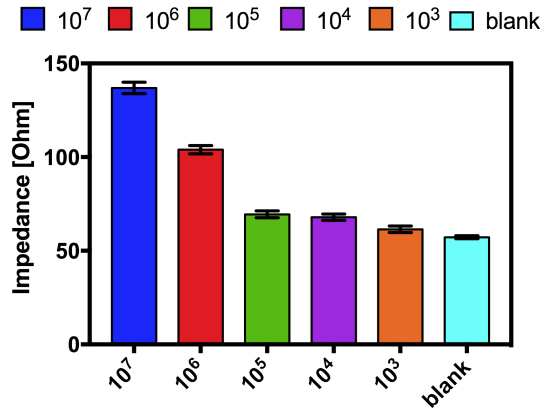

(a)

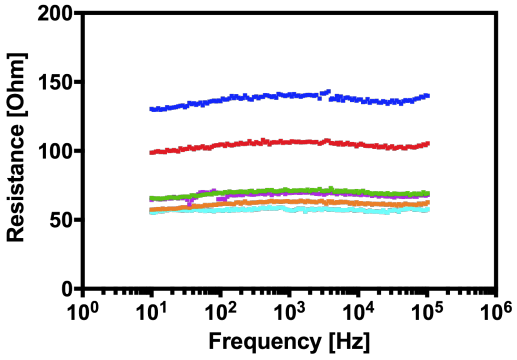

(b)

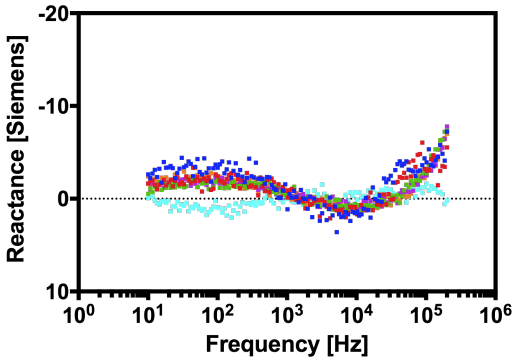

(c)

Figure 4.10: In vitro impedance spectroscopy of mammalian cells: **(a)** impedance results **(a)** real part and **(a)** imaginary part of measured electrical impedance of various cell concentrations.

decomposition of tissue based on freezing and sequential thawing resulted in a resistance decrease from 2135.75 ± 9.93 Ohm to 881.97 ± 33.97 Ohm at a frequency of 10 Hz. Similar decrease thus characteristic dispersion behaviour for intact and compromised tissue was observable between 10 Hz and 300 kHz. In the frequency range below 100 Hz the impedance sensing device was most sensitive for the resistive part of tissue decomposition. At frequencies above 100 Hz the sensitivity was declining. At a frequency above 300 kHz no difference between intact and decomposed tissue was observable for resistance. On the other hand, decrease in reactance due to membrane disruption during tissue degradation was detectable in the frequency range of 100 Hz to 300 kHz with a maximum sensitivity at 5 kHz corresponding to a reactance drop from -518.32 ± 11.29 Siemens to -45.91 ± 3.78 Siemens as shown in Figure 4.11b. Buffered saline solutions did not result in any characteristic dispersion. This means that the freezing protocol can effectively simulate tissue degradation resulting in disruption of cell membranes thus dielectric properties of tissues. This characteristic is well known in the scientific community and has already been used especially in food sciences and engineering [Wu et al., 2008].

4.5.3 Enzymatic Degradation of Tissue

To compare physical with biochemical degradation processes, chicken heart samples were subjected to enzymatic digestion for 24 hours using a sterile trypsin containing NaCl solution as depicted in Figure 3.7. In the course of trypsinization, heart tissue samples exhibit characteristic alteration in the impedance spectra caused by the degradation of cell membranes and both morphological and compositional changes within intra- and extracellular space. Figure 4.12 shows the impact of enzymatic degradation on the electric properties of chicken heart samples with a decrease of resistance over the whole frequency range from 10 Hz to 500 kHz with the highest

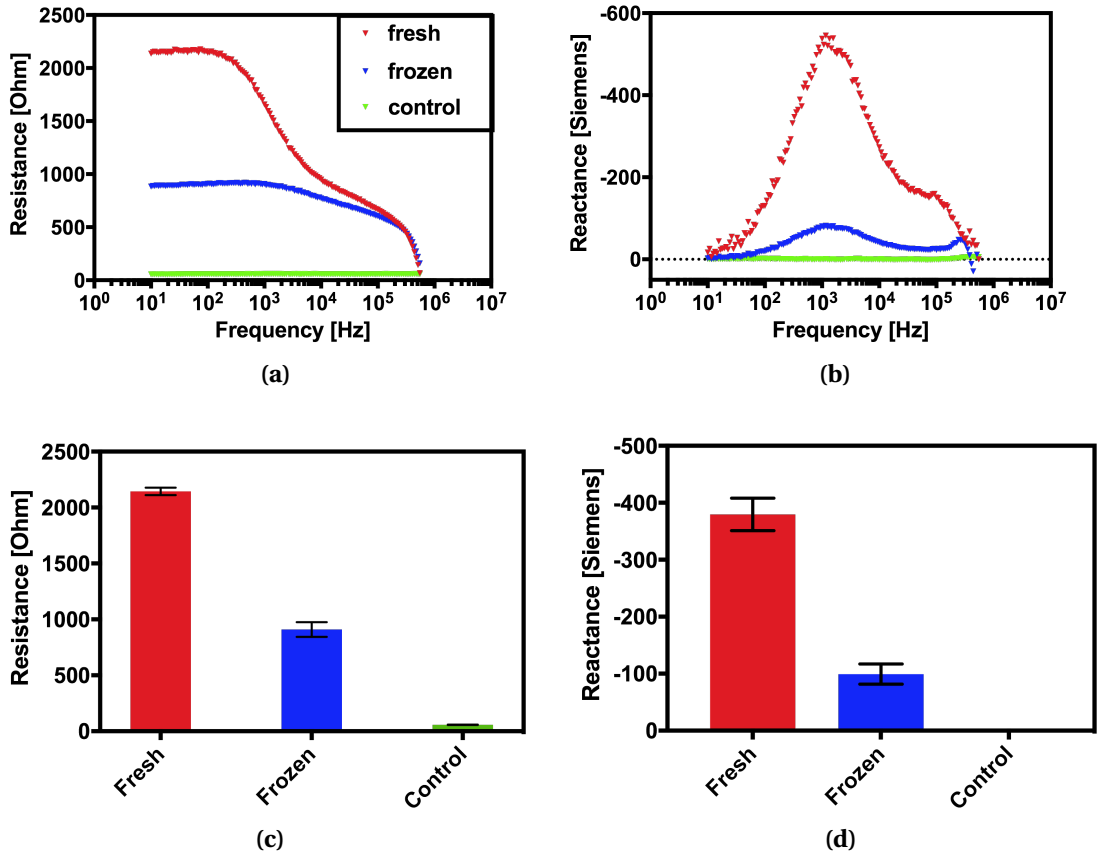

Figure 4.11: [Experimental simulation of changes in morphological integrity of chicken heart tissue: **(a)** Real and **(b)** imaginary spectra of measured electrical impedance for fresh and treated tissue samples. **(c)** and **(d)** show an average of resistance and reactance of measured freeze-treated samples at charactersitic frequencies of 100 Hz and 5 kHz, respectively. (n=4)

amplitude around 100 Hz. Even at a frequency of 500 kHz, a difference in resistance between non-compromised and enzymatically digested tissue was detectable. For reactance, the highest sensitivity was observable at 5 kHz and decomposition was readily detectable up to 500 kHz. Overall, change in reactance upon enzymatic degradation of tissue was detectable above 100 Hz, which is on close relation to the results obtained for freeze-treated heart samples as shown in 4.11. Compared to the saline solution controls, both tissue decomposition strategies are corresponding well with simulation data and the sensing device can readily distinguish between healthy and compromised organ tissue.

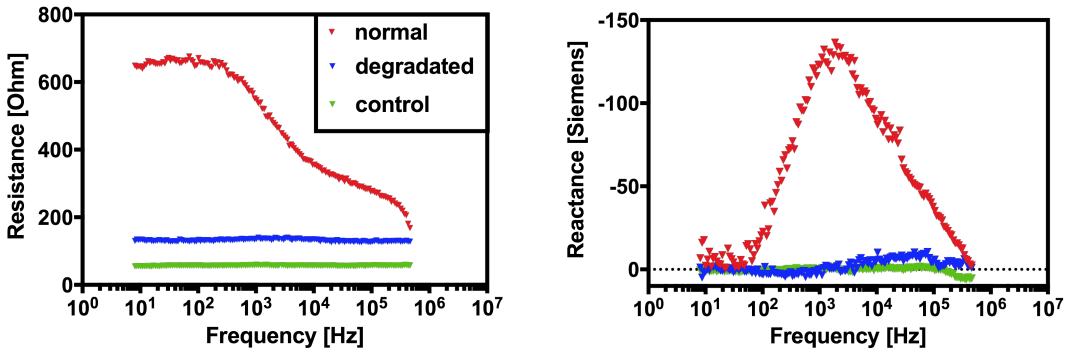

Figure 4.12: Enzymatic degradaton of chicken heart samples: **(a)** Real and **(b)** imaginary part of measured electrical impedance for fresh and treated tissue samples.

4.5.4 Continuous Monitoring of Morphological Tissue Integrity

Figure 4.13a and b show three-dimensional spectra of resistance and reactance over frequency and time. Gradual decline of resistance and capacitive reactance was observable at a characteristic frequency of 100 Hz and 5 kHz, respectively, being in line with previous results employing both computer simulation and freeze-treatment as well as enzymatic decomposition. Decline in resistance can be monitored over the whole frequency range, whereas for reactance frequencies below 100 Hz result in a flatline like values for saline solutions. At 100 Hz resistance declines from 670.80 Ohm to 133.30 Ohm. At 5 kHz capacitive reactance decreases over 24 hours from 127.47 ± Siemens to 3.36 ± Siemens. In addition, Figure 4.13c shows the decline in reactance in a biological tissue for a dynamic enzymatic decomposition process over a period of 24 hours compared to a blank trypsin solution without any capacitive membranes.

Even though an enzymatic decomposition of heart tissue might not be entirely comparable with a cardiac rejection process, continuous monitoring of changes in morphological tissue integrity is a necessary feature in order to detect signs of an onset of rejection.

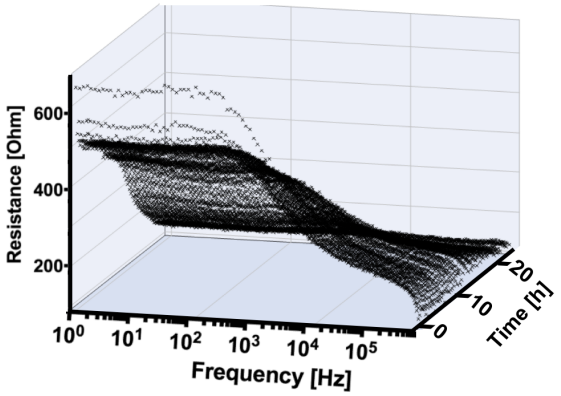

(a)

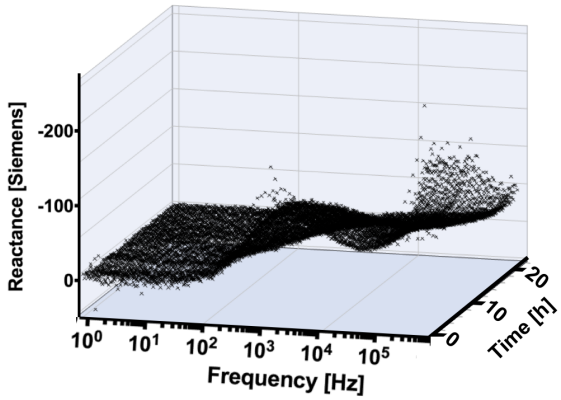

(b)

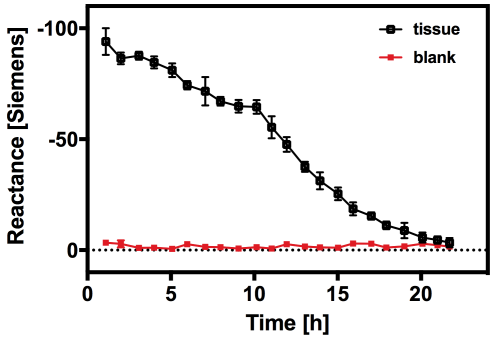

(c)

Figure 4.13: Continuous monitoring of structural changes in morphological tissue integrity caused by enzymatic degradation. **(a)** and **(b)** show the real and imaginary part of the imaginary impedance spectra over time, respectively. **(c)** shows a gradual decline of reactance at a characteristic frequency of 5 kHz.

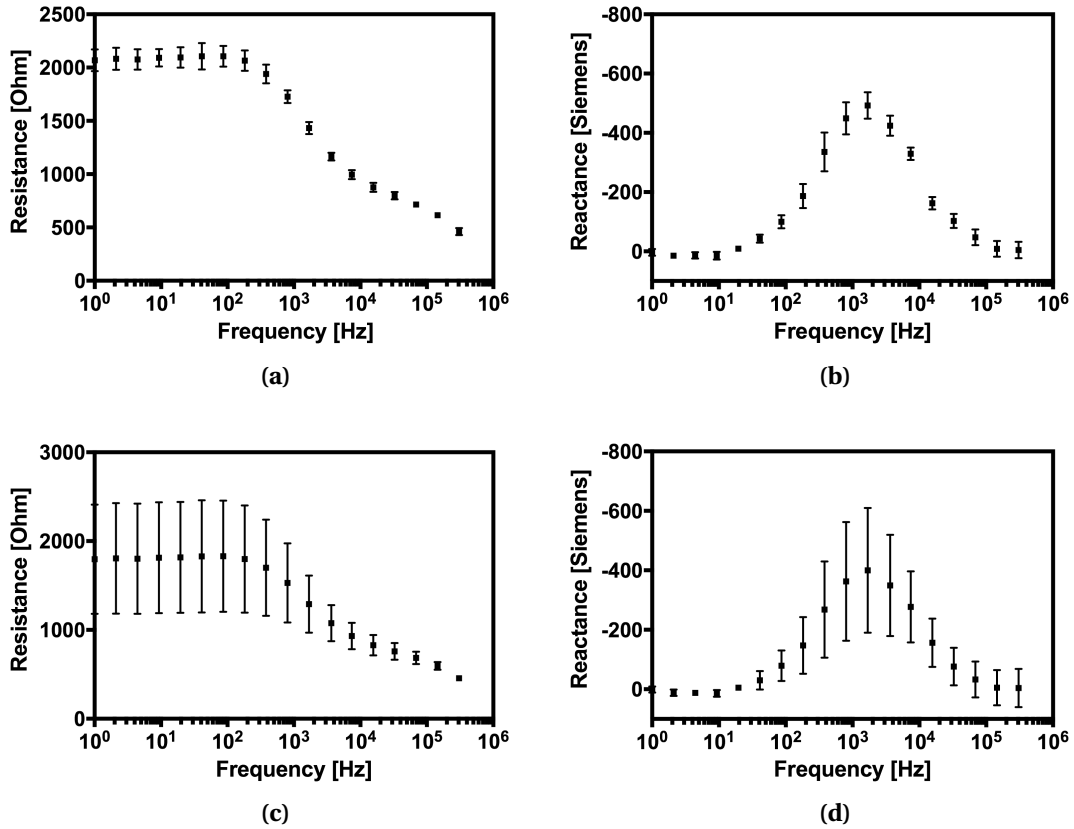

Figure 4.14: Variation of impedance signal within the same tissue sample: **(a)** real and **(b)** imaginary impedance spectra of chicken heart sample measured on various sensor positions in tissue and **(c)** real and **(d)** imaginary impedance of measured electrical impedance in various chicken heart samples. (n=5)

4.5.5 Deviation in Impedance Results

In order to evaluate whether the position of the sensor in tissue has an influence on the impedance results, the exact same tissue sample was measured using the same electrode setup several times on different positions. As shown in Figure 4.14a and b, there is just a negligible standard deviation in both real and imaginary impedance spectra of a chicken heart sample measured on various sensor positions. This may have been caused by a slightly variation in heart tissue structure and by the local tissue damage caused by the electrode itself. Although a slightly deviation was expected

due to a variation in size an age of the samples, a surprisingly high deviation between chicken heart tissue samples with almost identical properties was found in both real and imaginary part of the impedance signal as shown in Figure 4.14c and d, respectively. In spite of the high deviation, a characteristic β dispersion is still apparent. The resistance of a biological tissue is mostly influenced by the extracellular passive electrical properties at lower frequency and therefor, at frequencies below 1 kHz, there is a high deviation of resistance, whereas the imaginary part is predominantly affected by cell membrane and gap junction reactance, that is based on previous simulation results shown in 4.8, highly sensitive at about 1 kHz. On one hand, it should be noted that the sensor will be implemented at the time of transplantation and there is neither an intention to differentiate between different tissue samples, nor will the sensor be moved once implanted. On the other hand, these results support the premise that passivated electrical impedance spectroscopy is highly sensitive to even small structural diversities in tissue properties.

4.5.6 In vivo Myocardial Impedance Analysis

As can be seen in Figure 3.8, implantation of sensor prototype in a beating heart was succesfuly performed. However, despite the flexible substrate and a careful surgical operation, due to an excessive beating movement and a measured heart rate of over 90 bpm, the electrodes have still caused a considerable tissue damage, that has lead to minor bleeding. We must keep in mind, that any alteration in morphological tissue integrity may affect measured myocardial impedance and therefor, a damage caused by the sensor itself should be minimized. Nevertheless, Figure 4.15a and b show spectra of measured in vivo myocardial resistance and reactance over a frequency sweep from 100 Hz to 1 MHz in a beating heart. It can be easily recognized, that the Keysight LCZ meter, which has been used during measuring in vivo myocardial

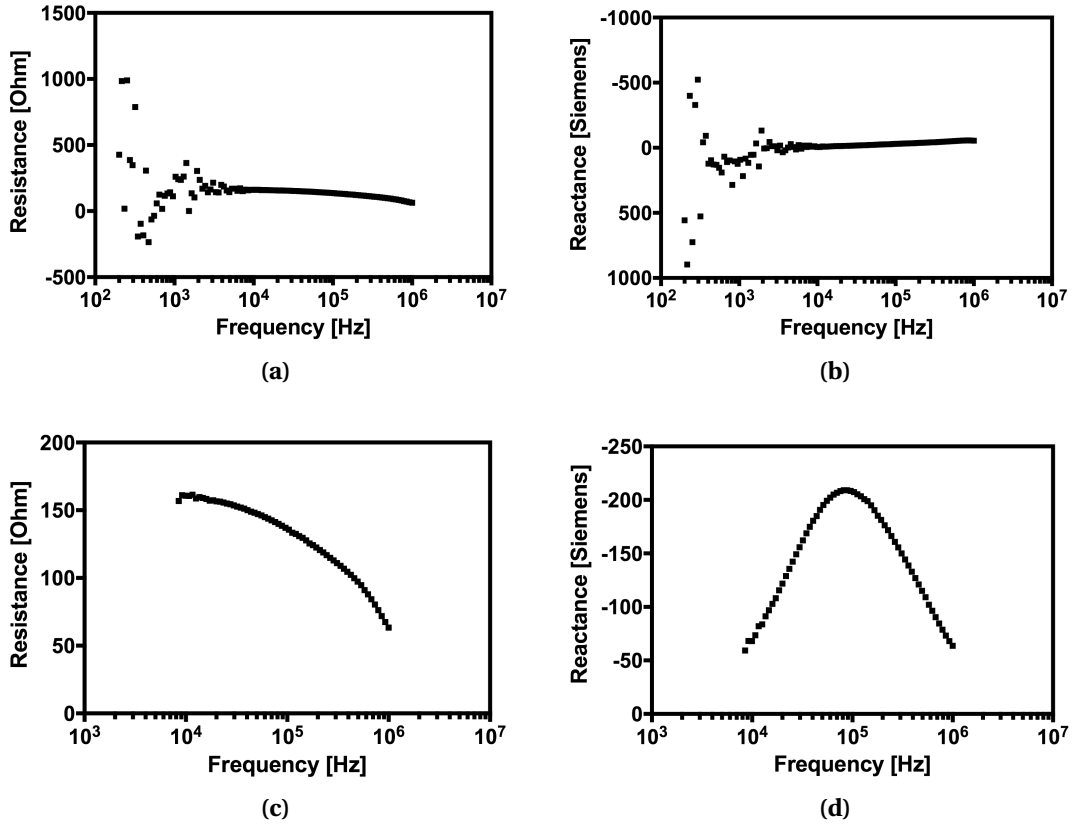

Figure 4.15: Results of in vivo myocardial impedance measurement over a frequency sweep between 100 Hz and 500 kHz: measured in vivo **(a)** real and **(b)** imaginary impedance. **(c)** and **(d)** show both corrected real and imaginary part of measured electrical impedance.

impedance, has a discernible influence on both resistance and reactance results at frequencies below 5 kHz leading to obviously unfeasible results within this area. Compared to previous results in Figure 4.12 and Figure 4.11, this can be seen as an instrument error. Figure 4.15c and d show the corrected spectra of in vivo myocardial resistance and reactance, respectively. Results below 5 kHz were excluded and results were corrected using a correction function, that has been explained in detail in Chapter 4.4. Despite the cut-off in measurement values at lower frequencies, in Figure 4.15c, a developed β dispersion can be found with a decrease of resistance from 161,34 Ohm to 63,35 Ohm over the corrected frequency range. These values are slightly lower than previous measurement results in Figure 4.12 and Figure 4.11, however based

on the variation, that has been shown between various samples in Figure 4.14, these results seem to be acceptable. In Figure 4.15d, a characteristic peak was detectable with a maximum sensitivity at 100 kHz corresponding to a peak value of -288.99 Siemens, compared to both previous in silico simulation and ex vivo tissue impedance experiments, where the maximum in reactance was detected at 5 kHz. Both in vivo resistance and reactance seem to be shifted towards higher frequencies, that may be also based on the fact, that another instrument was used for these experiments. In general, beside the additional mechanical stress, heart beating does not seem to affect myocardial impedance values. In order to evaluate whether a non-drifting in

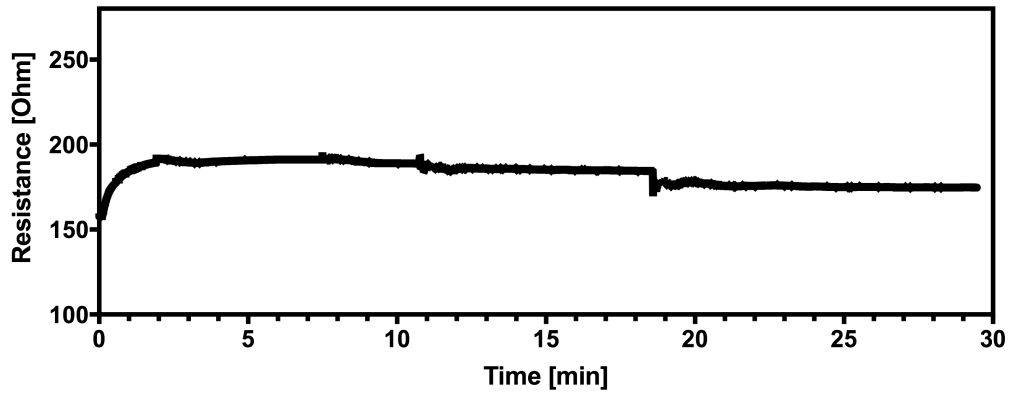

(a)

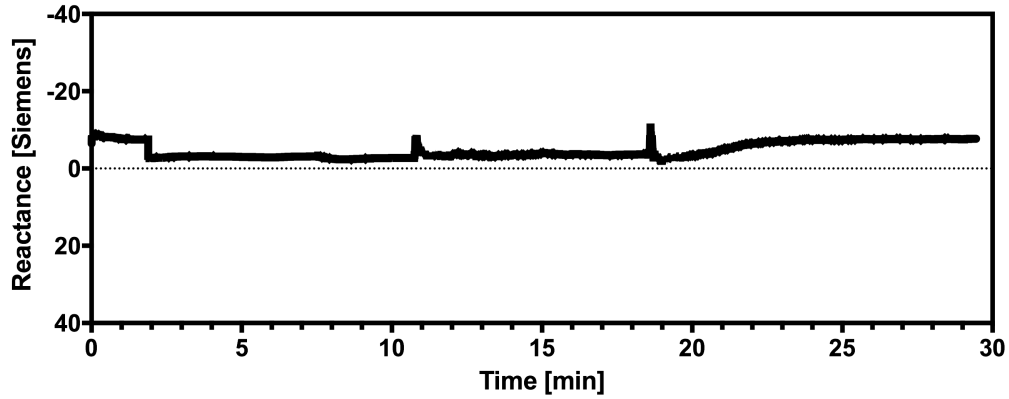

(b)

Figure 4.16: Results of continuous in vivo myocardial impedance measurement at 10 kHz: measured in vivo **(a)** real and **(b)** imaginary impedance. Due to computation reasons, seperate single measurements have been jointed together in order to maintain a time-resolved spectra.

vivo myocardial impedance analysis was possible in a beating heart, a continuous measurement was performed at 10 kHz[1]. Based on computational reasons, three single impedance measurement results have been jointed together. Since there was no break between these measurements, these spectra presented in Figure 4.16 can be seen as continuous. However, as can be seen after 11 and 18 minutes, outliers appear within both resistance and reactance spectra, that are clearly associated with triggering a new impedance measurement and hence sudden changes in voltage. In Figure 4.16a, resistance shows a slightly increase after implantation of the sensor, that may be based on the physical damage and bleeding caused by the cardiac surgeon. Right after the surgical intervention, the implanted sensor is immersed in and surrounded by blood, that has a high concentration of ionic compounds that artifically lower electrical impedance signal. After some minutes, the bleeding was stopped and a continuous myocardial signal was detected. There is a sligtly drifting and decline in resistance signal over time, that may be caused by heart beating and a continuous tissue damage and bleeding during measurement. Unfortunately, the experiment was performed at 10 kHz instead of the shifted optimal frequency of 100 kHz and therefor, a very low reactance signal was detected as shown in Figure 4.16b, that cannot be used for any further investigation. However, based on the results in Figure 4.15, a much higher reactance signal can be expected at 100 kHz.

[1] Since based on the previous results, a peak in reactance signal between 1 and 10 kHz was expected, there has been no in vivo measurement performed at 100 kHz, unfortunately.

5 Conclusions and Future Work

Heart failure is the largest cause of hospitalization and for many of those patients, there is no other option left, but to undergo a heart transplantation. An implantable biosensor for transplant rejection would provide for the first time the opportunity to continuously assess transplant performance over long periods of time and might replace endomyocardial biopsies permanently.

Based on its widespread and successful application in medical implants and the intention to detect and monitor cardiac graft rejection over a long period of time, passivated titanium electrodes with an insulating dioxide surface were successfully fabricated using a thermal passivation technology. In order to meet the requirements of a flexible implant, that resist an extraordinary mechanical stress of contraction events and fits the curvilinear surface of anhuman heart, inkjet printed bendable circuits on a PDMS substrate were succesfully used to replace conventional wiring of the implanted sensor. In addition to its biocompatible properties, using a PDMS based device with a linear array of four electrodes with a constant interelectrode distance in a tetrapolar configuration, electrode/tissue interface impedance could been minimized by a complete sensor isolation, that results in a physical removal of the

impedance electrodes from the liquid sensing environment and therefor eliminates ohmic contributions, bubble formation and electrode polarization events providing a non-drifting measurement condition over a long period of time. In scope of this thesis, no long-term experiments could been carried out, hence this hypothesis should to be examined in a long-term in vivo animal test over weeks. In addition to that, also long-term biocompatibility studies are desirable in order to analyze encapsulation processes of the sensor and healing of surgical damage, that may be caused during implantation of the device. During in vivo experiments, a minor injury and bleeding of the myocardial tissue were visible that may be caused by the electrode itself in a beating heart. In order to reduce this in vivo tissue injury, an even more flexible, titanium dioxide coated, polymeric microneedle electrodes have been proposed for further development.

In the course of cardiac rejection, myocardial tissue exhibits characteristic changes in the electrical impedance spectra mainly caused by the inflammatory infiltration of immune cells and both morphological and compositional changes within the intra- and extracellular space, that is based in based on distinct relaxation modes that occur in a multicellular system. Using passivated electrodes, discrete and continuous myocardial tissue impedance results with a sufficient accuracy could been achieved with respect to all necessary safety requirements. Developing the presented sensing device employing biocompatible electrodes, we achieved to detect similar changes in tissue characteristics and clearly distinguish between normal and alterated morphological tissue integrity. The amount of decrease in capacitive reactance within the β dispersion region is a straightforward and effective method to detect these electrophysiologically changes and therefor it makes sense to use this technology in order to monitor acute and chronic cardiac allograft rejection without any additinal surgical invasive treatment. Even though in vivo myocardial impedance analysis results were

negatively affected by instrumental errors, it could been shown, that a satisfactory and stabile results could been achieved using passivated electrodes in a contracting heart. In order to impedimetrically map a single cardiac cycle, that may be an interesting feature in order to analyse rejection processes, an adequate amont of measurement points and hence a sample rate below 30 ms are necessary.

The ability to differentiate between healthy and pathological tissue environment is just the minimum requirement for analyzing a rejection process. Additionally, we were also able to continuously and impedimetrically monitor structural changes in morphological tissue integrity over time, which is a key advantage compared to the current golden standard. Even though there was no exact in vivo or in vitro rejection model available in scope of this work, both physical and biochemical degradation processes resulting in a disturbed and alterated tissue environment have showed detectable electrophysical changes, which are comparable with expected results in a rejected tissue.

In order to answer remaining scientific questions, we envision applying the presented impedimetric sensing device for tissue rejection monitoring in a rabbit in vivo model. Since wired electrode connections are a frequent problem in animal studies and test subjects need to be sedated during the experiment in order to avoid self-harm of the animals by scratching, a replacement of the conventional wired connections to the analysis system are necesarry through RFID technology for wireless communication between the sensing device and the impedance measurement unit. Based on the ability to continuously monitor the status of an implanted heart, the efficacy of a medical treatment by using immunosupressors may also be evaluated through the proposed passivated impedance technology.

A Appendix

A.1 List of Materials

Table A.1: List of Equipments

#	Label	Manufacturer
1	VMP3/P-01 Potentiostat	Bio Logic, France
2	E4980AL Precision LCR Meter	Keysight, USA
3	Supra40 SEM	Zeiss, Germany
4	Lab centrifuge	Eppendorf, Germany
5	Spin Coater	Laurell Tech. Corp., USA
6	Dimatix inkjet printer 2831 series	FujiFilm, Japan
7	Digital multimeter IDM67	Isotech, Austria
8	Air plasma system	BlackHole-Lab, France
9	CNC laser cutter	Universal Laser Systems, USA
10	Mini incubator	Labnet, USA
11	CO2 Incubator	Binder, USA
12	Fridge, cell culture media	Gorenje, Slovenia
13	Pipettes, P20, P100, P1000	Gilson, USA
14	Heating magnetic stirrer	UniEquip, Germany
15	Laminar flow hood	Thermo Fisher Scientific, USA

Table A.2: List of Chemicals

#	Label	Manufacturer
1	Titanium wire, Grade 1 (99.5 %) 0.49 mm	Solution Materials, USA
2	Potassium hexacyanoferrate(II) trihydrate	Sigma-Aldrich, Germany
3	Phosphate-Buffered-Saline 10X, pH=7.4	Sigma-Aldrich, Germany
4	PDMS	Sylgard 184, Dow Corning, USA
5	(3-mercaptopropyl)trimethoxysilane	abc GmbH, Germany
6	HCl	Sigma-Aldrich, Germany
7	Tetrahydrofuran	Sigma-Aldrich, Germany
8	2-Propanol	Sigma-Aldrich, Germany
9	Silver conductive ink	ANP Silverjet DHP 40LT-A, South Korea
10	Conductive silver paste	Sigma-Aldrich, Germany
11	Sodium chloride 99 %, AR grade	Sigma-Aldrich, Germany
12	Jurkat cell line, ATCC, TIB-152	Ertl Group, Austria
13	RPMI 1640 media	BioWhittaker, USA
14	Fetal calf serum	Biowest, USA
15	Antibiotic-antimycotic solution	Biowest, USA
16	Trypsin solution	Sigma-Aldrich, Germany

A.2 Python Codes for Keysight E4980AL

A.2.1 Logarithmic Frequency Sweep

```
import visa

import numpy as np

from matplotlib import pyplot as plt

import re

import sys

import os


def print_usage():

print("Correct usage:")
```

```
print("  default:")
print("    frequency_sweep_impedance.py file_name")
print("      file_name: name of file to store data")
print("  custom:")
print("    frequency_sweep_impedance.py file_name fi ff voltage
num_of_samples")
print("      file_name: name of file to store data")
print("      fi: initial frequency")
print("      ff: final frequency")
print("      voltage: fixed voltage")
print("      num_of_samples: number of samples to average")
exit()

if len(sys.argv) != 2 and len(sys.argv) != 6:
print_usage()

file_name = sys.argv[1]
if os.path.exists(file_name):
print("File already exists: " + file_name)
overwrite = raw_input("Overwrite? (y/n) ")
if overwrite != "y":
exit()

fi = 20
ff = 2000
voltage = 0.1
```

```
num_of_samples = 1


if len(sys.argv) == 6:
fi = int(sys.argv[2])
ff = int(sys.argv[3])
voltage = float(sys.argv[4])
num_of_samples = int(sys.argv[5])


rm = visa.ResourceManager()
inst = rm.open_resource(rm.list_resources()[0])
print("Connected to: ")
print(inst.query("*IDN?"))


samples_per_decade = 30
log_fi = np.log10(fi)
log_ff = np.log10(ff)
decades = log_ff - log_fi
freq_list = np.logspace(log_fi, log_ff, num = decades*samples_per_decade)


print("Starting a frequency sweep from " + str(freq_list[0]) + "-"
+ str(freq_list[-1]))


inst.write(":VOLTage:LEVel " + str(voltage))
print("Voltage set to: " + str(voltage))


r_list = []
```

```
x_list = []

z_list = []

d_list = []

for freq in freq_list:

r_samples = []

x_samples = []

z_samples = []

d_samples = []

for i in range(num_of_samples):

inst.write(":FREQuency:CW " + str(freq))

inst.write(":FUNCtion:IMPedance:TYPE RX")

inst.write(":TRIGger:IMMediate")

#imped = inst.query(":FETCh:IMPedance:CORRected?")

rx = inst.query(":FETCh:IMPedance:FORMatted?")

#print(imped)

m = re.search("(.+),(.+),.+", rx)

if m:

# By experimentation units are in ohms

r = float(m.group(1))

x = float(m.group(2))

r_samples.append(r)

x_samples.append(x)

else:

print("Unrecognized output: " + str(rx))

exit()
```

```
inst.write(":FUNCtion:IMPedance:TYPE ZTD")
inst.write(":TRIGger:IMMediate")
ztd = inst.query(":FETCh:IMPedance:FORMatted?")
#print(imped)
m = re.search("(.+),(.+),.+", ztd)
if m:
# By experimentation units are in ohms
z = float(m.group(1))
d = float(m.group(2))
z_samples.append(z)
d_samples.append(d)
else:
print("Unrecognized output: " + str(ztd))
exit()

r_list.append(np.mean(r_samples))
x_list.append(np.mean(x_samples))
z_list.append(np.mean(z_samples))
d_list.append(np.mean(d_samples))

f = open(file_name, "w")
f.write("Frequency, R, X, Z, Phase\n")
for i in range(len(freq_list)):
f.write(str(freq_list[i]) + ", " + str(r_list[i]) + ", "
+ str(x_list[i]) + ", " + str(z_list[i]) + ", " + str(d_list[i]) + "\n")
f.close()
```

```
fig, ax1 = plt.subplots()
ax1.scatter(freq_list, r_list, label="real", color="b")
ax1.set_xlabel('Frequency (Hz)')
ax1.set_ylabel("Ohms", color="b")
ax1.tick_params('y', colors="b")

ax2 = ax1.twinx()
ax2.scatter(freq_list, x_list, label="imag", color="r")
ax2.set_ylabel("Siemens", color="r")
ax2.tick_params('y', colors="r")

plt.xlim(fi, ff)
plt.xscale("log")
plt.show()
```

A.2.2 Continuous Impedance Spectroscopy at a Choosen Frequency

```
import visa
import numpy as np
import re
import sys
import os
import datetime
```

```
def print_usage():
print("Correct usage:")
print("  continuous_impedance.py frequency file_name")
print("    file_name: name of file to store data")
exit()

if len(sys.argv) != 3:
print_usage()

freq = sys.argv[1]

# Do not overwrite a file if it already exists
file_name = sys.argv[2]
if os.path.exists(file_name):
print("File already exists: " + file_name)
overwrite = raw_input("Overwrite? (y/n) ")
if overwrite != "y":
exit()

voltage = 0.1
num_of_samples = 1

rm = visa.ResourceManager()
inst = rm.open_resource(rm.list_resources()[0])
print("Connected to: ")
print(inst.query("*IDN?"))
```

```
inst.write(":VOLTage:LEVel " + str(voltage))
print("Voltage set to: " + str(voltage))

inst.write(":FREQuency:CW " + freq)
print("Frequency set to: " + freq)

r_samples = []
x_samples = []
z_samples = []
d_samples = []
# Open file for writing
f = open(file_name, "w")
f.write("Timestamp, Frequency, R, X, Z, Phase\n")
# Loops forever, must be killed using ^C
while True:
for i in range(num_of_samples):
inst.write(":FUNCtion:IMPedance:TYPE RX")
inst.write(":TRIGger:IMMediate")
#imped = inst.query(":FETCh:IMPedance:CORRected?")
rx = inst.query(":FETCh:IMPedance:FORMatted?")
#print(imped)
m = re.search("(.+),(.+),.+", rx)
if m:
# By experimentation units are in ohms
r = float(m.group(1))
```

```
x = float(m.group(2))
r_samples.append(r)
x_samples.append(x)
else:
print("Unrecognized output: " + str(rx))
exit()

inst.write(":FUNCtion:IMPedance:TYPE ZTD")
inst.write(":TRIGger:IMMediate")
ztd = inst.query(":FETCh:IMPedance:FORMatted?")
#print(imped)
m = re.search("(.+),(.+),.+", ztd)
if m:
# By experimentation units are in ohms
z = float(m.group(1))
d = float(m.group(2))
z_samples.append(z)
d_samples.append(d)
else:
print("Unrecognized output: " + str(ztd))
exit()

# Write timestamp
f.write(str(datetime.datetime.now()))
f.write(", ")
f.write(str(np.mean(r_samples)))
```

```
f.write(", ")

f.write(str(np.mean(x_samples)))

f.write(", ")

f.write(str(np.mean(z_samples)))

f.write(", ")

f.write(str(np.mean(d_samples)))

f.write("\n")


f.close()
```

Bibliography

Abassi, Y. A., Jackson, J. A., Zhu, J., Oconnell, J., Wang, X., and Xu, X. (2004). Label-free, real-time monitoring of IgE-mediated mast cell activation on microelectronic cell sensor arrays. *Journal of Immunological Methods*, 292(1-2):195–205.

Ahn, H., Shin, H., Yun, S., Kim, J., and Choi, J. (2005). Measurement of bioimpedance and cell viability during ischemia-reperfusion in the rat liver. *Conference proceedings : ... Annual International Conference of the IEEE Engineering in Medicine and Biology Society. IEEE Engineering in Medicine and Biology Society. Annual Conference*, 2:1945–7.

Balazic, M., Kopac, J., Jackson, M. J., and Ahmed, W. (2007). Review : titanium and titanium alloy applications in medicine. *International Journal of Nano and Biomaterials*, 1(1):3–34.

Bard, a. and Faulkner, L. (2002). Allen J. Bard and Larry R. Faulkner, Electrochemical Methods: Fundamentals and Applications, New York: Wiley, 2001. *Russian Journal of Electrochemistry*, 38(12):1505–1506.

Barnard, C. N. (1967). The operation. A human cardiac transplant: an interim report of a successful operation performed at Groote Schuur Hospital, Cape Town. *South African medical journal = Suid-Afrikaanse tydskrif vir geneeskunde*, 41(48):1271–1274.

Bhat, S. and Kumar, A. (2013). Biomaterials and bioengineering tomorrow's healthcare. *Biomatter*, 3(3):1–12.

Blad, B. and Baldetorp, B. (1996). Impedance spectra of tumour tissue in comparison with normal tissue; a possible clinical application for electrical impedance tomography. *Physiol Meas.*, 17 Suppl 4(0967-3334 (Print)):A105–A115.

Bohinc, K., Shrestha, A., Brumen, M., and May, S. (2012). Poisson-Helmholtz-Boltzmann model of the electric double layer: Analysis of monovalent ionic mixtures. *Physical Review E - Statistical, Nonlinear, and Soft Matter Physics*, 85(3).

Bragós, R., Gámez, X., Cairó, J., Riu, P. J., and Gòdia, F. (1999). Biomass monitoring using impedance spectroscopy. In *Annals of the New York Academy of Sciences*, volume 873, pages 299–305.

Buendia, R., Seoane, F., and Gil-Pita, R. (2010). A novel approach for removing the hook effect artefact from Electrical Bioimpedance spectroscopy measurements. *Journal of Physics: Conference Series*, 224(1):012126.

Bui, A. L., Horwich, T. B., and Fonarow, G. C. (2011). Epidemiology and risk profile of heart failure. *Nat Rev Cardiol*, 8(1):30–41.

Cheng, I. C. and Wagner, S. (2009). Overview of flexible electronics technology. In *Flexible Electronics*, volume 11, pages 1–28. Elsevier.

Christie, J. D., Edwards, L. B., Kucheryavaya, A. Y., Benden, C., Dipchand, A. I., Dobbels, F., Kirk, R., Rahmel, A. O., Stehlik, J., and Hertz, M. I. (2012). The registry of the international society for heart and lung transplantation: 29th adult lung and heart-lung transplant report - 2012. *Journal of Heart and Lung Transplantation*, 31(10):1073–1086.

Cole, K. S. (1940). PERMEABILITY AND IMPERMEABILITY OF CELL MEMBRANES FOR IONS. *Cold Spring Harbor Symposia on Quantitative Biology*, 8(0):110–122.

Cook, C., Cole, G., Asaria, P., Jabbour, R., and Francis, D. P. (2014). The annual global economic burden of heart failure. *International Journal of Cardiology*, 171(3):368–376.

Costa, E. L., Lima, R. G., and Amato, M. B. (2009). Electrical impedance tomography. *Current Opinion in Critical Care*, 15(1):18–24.

Costello, J. P., Mohanakumar, T., and Nath, D. S. (2013). Mechanisms of chronic cardiac allograft rejection. *Texas Heart Institute Journal / from the Texas Heart Institute of St. Luke's Episcopal Hospital, Texas Children's Hospital*, 40(4):395–399.

Cybulski, G., Strasz, A., Niewiadomski, W., and Gąsiorowska, A. (2012). Impedance cardiography: recent advancements. *Cardiology journal*, 19(5):550–6.

Dandel, M., Hummel, M., Muller, J., Wellnhofer, E., Meyer, R., Solowjowa, N., Ewert, R., and Hetzer, R. (2001). Reliability of Tissue Doppler Wall Motion Monitoring After Heart Transplantation for Replacement of Invasive Routine Screenings by Optimally Timed Cardiac Biopsies and Catheterizations. *Circulation*, 104(Supplement 1):I–184–I–191.

Dean, D. A., Ramanathan, T., Machado, D., and Sundararajan, R. (2008). Electrical impedance spectroscopy study of biological tissues. *Journal of Electrostatics*, 66(3-4):165–177.

Domachuk, P., Tsioris, K., Omenetto, F. G., and Kaplan, D. L. (2010). Bio-microfluidics: Biomaterials and biomimetic designs.

Du, K., Wathuthanthri, I., Liu, Y., Xu, W., and Choi, C. H. (2012). Wafer-scale pattern

transfer of metal nanostructures on polydimethylsiloxane (PDMS) substrates via holographic nanopatterns. *ACS Applied Materials and Interfaces*, 4(10):5505–5514.

Feng, B., Weng, J., Yang, B., Chen, J., Zhao, J., He, L., Qi, S., and Zhang, X. (2002). Surface characterization of titanium and adsorption of bovine serum albumin. *Materials Characterization*, 49(2):129–137.

Ferreira, J., Seoane, F., and Lindecrantz, K. (2013). Portable bioimpedance monitor evaluation for continuous impedance measurements. Towards wearable plethysmography applications. In *Proceedings of the Annual International Conference of the IEEE Engineering in Medicine and Biology Society, EMBS*, pages 559–562.

Fishman, J. A. (2007). Infection in Solid-Organ Transplant Recipients. *New England Journal of Medicine*, 357(25):2601–2614.

Frazier, A., Chen, Z., and Han, A. (2009). Whole-Cell Impedance Analysis for Highly and Poorly Metastatic Cancer Cells. *Journal of Microelectromechanical Systems*, 18(4):808–817.

From, A. M., Maleszewski, J. J., and Rihal, C. S. (2011). Current Status of Endomyocardial Biopsy. *Mayo Clinic Proceedings*, 86(11):1095–1102.

Gabriel, C., Peyman, a., and Grant, E. H. (2009). Electrical conductivity of tissue at frequencies below 1 MHz. *Physics in medicine and biology*, 54(16):4863–4878.

Galanti, G., Stefani, L., Scacciati, I., Mascherini, G., Buti, G., Maffulli, N., Galanti, G., Stefani, L., Scacciati, I., Mascherini, G., Buti, G., and Stefani, L. (2015). Eating and nutrition habits in young competitive athletes: a comparison between soccer players and cyclists. *Translational medicine @ UniSa*, 11(8):44–7.

Galvani, L. (1791). De viribus electricitatis in motu muscularis commentarius. *De*

Bononiensi Scientiarum et Artium Instituto atque Academia Commentarii, 7:363–418.

Geddes, L. A. and Baker, L. E. (1967). The specific resistance of biological material-A compendium of data for the biomedical engineer and physiologist. *Medical and biological engineering*, 5(3):271–293.

Geddes, L. a. and Roeder, R. (2003). Criteria for the selection of materials for implanted electrodes. *Annals of Biomedical Engineering*, 31(7):879–890.

Gemelli, E., Scariot, A., and Camargo, N. H. A. (2007). Thermal characterization of commercially pure titanium for dental applications. *Material Research*, 10(3):241–246.

Giovinazzo, G., Ribas, N., Cinca, J., and Rosell-Ferrer, J. (2011). The feasibility of transoesophageal bioimpedance measurements for the detection of heart graft rejection. *Physiological measurement*, 32(7):867–76.

Grimnes, S. and Martinsen, Ø. G. (2015). *Bioimpedance and Bioelectricity Basics*. Elsevier.

Guilbault, G. G. and Hjelm, M. (1989). IUPAC Gold Book. *Pure and Applied Chemistry*, 61(9):1657–1664.

Heusler, K. E., Landolt, D., and Trasatti, S. (1989). Electrochemical corrosion nomenclature. (Recommendations 1988). *Pure and Applied Chemistry*, 61:19–22.

Hildebrandt, C., Büth, H., Cho, S., Impidjati, and Thielecke, H. (2010). Detection of the osteogenic differentiation of mesenchymal stem cells in 2D and 3D cultures by electrochemical impedance spectroscopy. *Journal of Biotechnology*, 148(1):83–90.

Höber, R. (1910). Eine Methode, die elektrische Leitfähigkeit im Innern von Zellen zu messen. *Pflüger's Archiv für die Gesammte Physiologie des Menschen und der Tiere*, 133(4-6):237–253.

Ivorra, A. (2005). *Contributions to the measurement of electrical impedance for living tissue ischemia injury monitoring*. PhD thesis, Universitat Politecnica de Catalunya.

Ivorra, A. (2013). Bioimpedance Monitoring for Physicians: An Overview. *Centre Nacional de Microelectrònica Biomedical Applications Group*, pages 1–35.

Jaffrin, M. Y. (2009). Body composition determination by bioimpedance: an update. *Current opinion in clinical nutrition and metabolic care*, 12(5):482–486.

Jamesh, M., Sankara Narayanan, T. S. N., and Chu, P. K. (2013). Thermal oxidation of titanium: Evaluation of corrosion resistance as a function of cooling rate. *Materials Chemistry and Physics*, 138(2-3):565–572.

Johnson, N. B., Hayes, L. D., Brown, K., Hoo, E. C., and Ethier, K. A. (2014). CDC National Health Report: leading causes of morbidity and mortality and associated behavioral risk and protective factors - United States, 2005-2013. *Morbidity and Mortality Weekly Report*, 63:3–27.

Ju, H. Y. and Park, J. K. (2005). Cytotoxicity test based on electrochemical impedance measurement of HepG2 cultured in microfabricated cell chip. *Analytical Biochemistry*, 341(2):308–315.

Khalil, S. F., Mohktar, M. S., and Ibrahim, F. (2014). The theory and fundamentals of bioimpedance analysis in clinical status monitoring and diagnosis of diseases. *Sensors (Switzerland)*, 14(6):10895–10928.

Khan, S., Lorenzelli, L., and Dahiya, R. S. (2015). Technologies for printing sensors and

electronics over large flexible substrates: A review. *IEEE Sensors Journal*, 15(6):3164–3185.

Kim, S. H., Moon, J. H., Kim, J. H., Jeong, S. M., and Lee, S. H. (2011). Flexible, stretchable and implantable PDMS encapsulated cable for implantable medical device. *Biomedical Engineering Letters*, 1(3):199–203.

Kindt, T., Goldsby, R., Osborne, B., and Kuby, J. (2007). Kuby immunology. *The Journal of experimental medicine*, 206(13):2925–35.

Kittleson, M., Patel, J., Rafiei, M., Osborne, A., Tittle, M., Chang, D. H., Czer, L., Esmailian, F., Trento, A., and Kobashigawa, J. (2017). Longer and Shorter Hospital Stay after Heart Transplant Both Risk Factors for Suboptimal Outcome. *The Journal of Heart and Lung Transplantation*, 32(4):S263.

Kochanek, K. (2016). Deaths: Final Data for 2014. *National Vital Statistics Reports*, 65(4).

Kumar, V., Abbas, A. K., Fausto, N., and Aster, J. C. (2009). *Kumar: Robbins and Cotran Pathologic Basis of Disease, Professional Edition, 8th ed.* Elsevier.

Kwasniak, P., Pura, J., Zwolinska, M., Wiecinski, P., Skarzynski, H., Olszewski, L., Marczak, J., Garbacz, H., and Kurzydlowski, K. (2015). Laser and chemical surface modifications of titanium grade 2 for medical application. *Applied Surface Science*, 336:267–273.

Lee, Y., Li, H., and Fonash, S. J. (2003). High-performance poly-Si TFT on plastic substrates using a nano-structured separation layer approach.

Liu, X., Chu, P., and Ding, C. (2004). Surface modification of titanium, titanium alloys, and related materials for biomedical applications. *Materials Science and Engineering: R: Reports*, 47(3-4):49–121.

Lund, L. H., Edwards, L. B., Kucheryavaya, A. Y., Benden, C., Christie, J. D., Dipchand, A. I., Dobbels, F., Goldfarb, S. B., Levvey, B. J., Meiser, B., Yusen, R. D., and Stehlik, J. (2016). The Registry of the International Society for Heart and Lung Transplantation: Thirty-first Official Adult Heart Transplant Report;2014; Focus Theme: Retransplantation. *The Journal of Heart and Lung Transplantation*, 33(10):996–1008.

Martin, S. T., Kato, T. S., Farr, M., McKeen, J. T., Cheema, F., Ji, M., Ross, A., Yerebakan, H., Naka, Y., Takayama, H., Restaino, S., Mancini, D., and Schulze, P. C. (2015). Similar Survival in Patients Following Heart Transplantation Receiving Induction Therapy Using Daclizumab vs. Basiliximab. *Circulation Journal*, 79(2):368–374.

McAdams, E. T., Lackermeier, A., McLaughlin, J. A., Macken, D., and Jossinet, J. (1995). The linear and non-linear electrical properties of the electrode-electrolyte interface. *Biosensors and Bioelectronics*, 10(1-2):67–74.

Melnik, E., Muellner, P., Bethge, O., Bertagnolli, E., Hainberger, R., and Laemmerhofer, M. (2014). Monolayer: Silanization of PDMS using MPTMS. *Chemical Communications*, 50:2424–2427.

Młyńczak, M. and Cybulski, G. (2012). Impedance pneumography: Is it possible? In *Proc. SPIE 8454, Photonics Applications in Astronomy, Communications, Industry, and High-Energy Physics Experiments 2012*, volume 8454, page 84541T.

Noszczyk-Nowak, A. (2009). Preliminary reference values for electrocardiography, echocardiography and myocardial morphometry in the European brown hare (Lepus europaeus). *Acta Veterinaria Scandinavica*, 51(6).

Nyberg, S. T., Fransson, E. I., Heikkila, K., Alfredsson, L., Casini, A., Clays, E., De Bacquer, D., Dragano, N., Ferrie, J. E., Goldberg, M., Hamer, M., Jokela, M., Karasek, R., Kittel, F., Knutsson, A., Koskenvuo, M., Nordin, M., Oksanen, T., Pentti, J., Rugulies,

R., Salo, P., Siegrist, J., Suominen, S. B., Theorell, T., Vahtera, J., Virtanen, M., Westerholm, P. J. M., Westerlund, H., Zins, M., Steptoe, A., Singh-Manoux, A., Batty, G. D., and Consortium, I.-W. (2013). Associations of job strain and lifestyle risk factors with risk of coronary artery disease: a meta-analysis of individual participant data. *CMAJ : Canadian Medical Association journal = journal de l'Association medicale canadienne*, 185(9):763–769.

Oldham, K. B. (2008). A Gouy-Chapman-Stern model of the double layer at a (metal)/(ionic liquid) interface. *Journal of Electroanalytical Chemistry*, 613(2):131–138.

Peyman, A., Gabriel, C., and Grant, E. H. (2007). Complex permittivity of sodium chloride solutions at microwave frequencies. *Bioelectromagnetics*, 28(4):264–274.

Pouilleau, J., Devilliers, D., Garrido, F., Durand-Vidal, S., and Mahé, E. (1997). Structure and composition of passive titanium oxide films. *Materials Science and Engineering: B*, 47(3):235–243.

Prodan, C., Mayo, F., Claycomb, J. R., Miller, J. H., and Benedik, M. J. (2004). Low-frequency, low-field dielectric spectroscopy of living cell suspensions. *Journal of Applied Physics*, 95(7):3754–3756.

Ratner, D., Brunette, D., Tengvall, P., Textor, M., and Thomsen, P. (2008). *Titanium in Medicine*. Elsevier.

Reitinger, S., Wissenwasser, J., Kapferer, W., Heer, R., and Lepperdinger, G. (2012). Electric impedance sensing in cell-substrates for rapid and selective multipotential differentiation capacity monitoring of human mesenchymal stem cells. *Biosensors and Bioelectronics*, 34(1):63–69.

Reza Atefi, S., Seoane, F., Thorlin, T., and Lindecrantz, K. (2013). Stroke damage detection using classification trees on electrical bioimpedance cerebral spectroscopy measurements. *Sensors (Switzerland)*, 13(8):10074–10086.

Schawn, H. (1957). Electrical properties of tissue and cell suspensions. *Adv. Biol. Med. Phys.*, 5:147–209.

Sethi, G. K., Kosaraju, S., Arabia, F. A., Roasdo, L. J., McCarthy, M. S., and Copeland, J. G. (1995). Is it necessary to perform surveillance endomyocardial biopsies in heart transplant recipients? *J Heart Lung Transplant*, 14(6 Pt 1):1047–1051.

Sticker, D. (2015). *Development of thiol-ene-epoxy thermoset microdevices with automated fluid handling and nanolayer passivated microstructured impedimetric sensor for in vitro cell-based assays*. PhD thesis, Technische Universität Wien.

Sticker, D., Rothbauer, M., Charwat, V., Steink??hler, J., Bethge, O., Bertagnolli, E., Wanzenboeck, H. D., and Ertl, P. (2015). Zirconium dioxide nanolayer passivated impedimetric sensors for cell-based assays. *Sensors and Actuators, B: Chemical*, 213:35–44.

Sun, J., Jiang, J., Bao, B., Wang, S., He, M., Zhang, X., and Song, Y. (2016). Fabrication of bendable circuits on a polydimethylsiloxane (PDMS) surface by inkjet printing semi-wrapped structures. *Materials*, 9(4).

Sun, T., Tsuda, S., Zauner, K.-P., and Morgan, H. (2010). On-chip electrical impedance tomography for imaging biological cells. *Biosensors & Bioelectronics*, 25(5):1109–1115.

Trebbels, D., Hradetzky, D., and Zengerle, R. (2009). Capacitive on-line hematocrit sensor design based on impedance spectroscopy for use in hemodialysis machines. In *Proceedings of the 31st Annual International Conference of the IEEE Engineering*

in Medicine and Biology Society: Engineering the Future of Biomedicine, EMBC 2009, pages 1208–1211.

Turner, A. (2013). Biosensors: Then and now.

Vert, M., Doi, Y., Hellwich, K.-H., Hess, M., Hodge, P., Kubisa, P., Rinaudo, M., and Schué, F. (2012). Terminology for biorelated polymers and applications (IUPAC Recommendations 2012). *Pure and Applied Chemistry*, 84(2):1.

Villares, A., Pera, G., Giner, I., Cea, P., López, M. C., and Martín, S. (2009). The Use of Cyclic Voltammetry To Probe the Passivation of Electrode Surfaces by Well-Ordered Self-Assembly and Langmuir–Blodgett Films. An Advanced Undergraduate Laboratory Experiment in Surface Science and Nanomaterials Chemistry. *Journal of Chemical Education*, 86(6):723.

Vine, S. M., Painter, P. L., Kuskowski, M. A., and Earthman, C. P. (2011). Bioimpedance spectroscopy for the estimation of fat-free mass in end-stage renal disease. *e-SPEN*, 6(1).

Wang, G., Li, J., Lv, K., Zhang, W., Ding, X., Yang, G., Liu, X., and Jiang, X. (2016). Surface thermal oxidation on titanium implants to enhance osteogenic activity and in vivo osseointegration. *Scientific Reports*, 6:31769.

Wang, Y., Ye, Z., and Ying, Y. (2012). New trends in impedimetric biosensors for the detection of foodborne pathogenic bacteria.

Webster, J. G., Clark, J. W., Neuman, M. R., Olson, W. H., Peura, R. A., Primiano, F. P., Siedband, M. P., and Wheeler, L. A. (2010). Medical instrumentation: Application and design. *Control Engineering Practice*, page 296.

Wegener, J., Keese, C. R., and Giaever, I. (2000). Electric cell-substrate impedance

sensing (ECIS) as a noninvasive means to monitor the kinetics of cell spreading to artificial surfaces. *Experimental cell research*, 259(1):158–166.

White, J. A., Guiraudon, C., Pflugfelder, P. W., and Kostuk, W. J. (1995). Routine surveillance myocardial biopsies are unnecessary beyond one year after heart transplantation. *J Heart Lung Transplant*, 14(6 Pt 1):1052–1056.

Wu, L., Ogawa, Y., and Tagawa, A. (2008). Electrical impedance spectroscopy analysis of eggplant pulp and effects of drying and freezing-thawing treatments on its impedance characteristics. *Journal of Food Engineering*, 87(2):274–280.

Wu, Y., Almasri, M., and Benson, J. D. (2011). MEMS Coulter counter for dynamic impedance measurement of cells. In *Proceedings of IEEE Sensors*, pages 794–797.

Xiao, C. and Luong, J. H. T. (2003). On-line monitoring of cell growth and cytotoxicity using electric cell-substrate impedance sensing (ECIS). *Biotechnology Progress*, 19(3):1000–1005.

Yin, Z. P., Huang, Y. A., Bu, N. B., Wang, X. M., and Xiong, Y. L. (2010). Inkjet printing for flexible electronics: Materials, processes and equipments.

TIBOR WLADIMIR

Mexikoplatz 25/2/24 ◇ A-1020, Vienna, Austria
(0043) · 660 · 4107816 ◇ tibor.wladimir@me.com

EDUCATION

University of Natural Resources and Applied Sciences, Vienna 2016 – 2018*
MSc. in Biotechnology *Vienna, AT*
Master's thesis: Development of an Implantable Biosensor for Rejection Detection and Long-term Monitoring in Cardiac Transplantation

University of Natural Resources and Applied Sciences, Vienna 2011 – 2015
BSc. in Food Sciences & Biotechnology *Vienna, AT*
Bachelor's thesis: Vector-borne Infectious Diseases and their Relevance for Human Health and Economy

Commercial High School 2010 – 2011
Vocational Baccalaureate Diploma *Oberwart, AT*

Vocational School for Tourism and Hospitality 2006 – 2008
Certificate of Apprenticeship in Professional Cookery *Altmünster, AT*

School of Hotel Management 2002 – 2006
High School Diploma *Debrecen, HU*

ADDITIONAL TRAINING AND STUDIES ABROAD

University of Hohenheim 07/2014
ELLS Summer University on Pathogens, Parasites and their Hosts *Stuttgart, DE*

Technische Universität Berlin 10/2013 – 04/2014
Exchange semester *Berlin, DE*

PUBLICATIONS AND SCHOLARSHIPS

Method for measuring the binding strength between cells and ligands in turbid solutions (co-inventor) DE 10 2014 210 590 (A1)

European Alpbach Forum Grant, 2017

Marshall Plan Scholarship, 2017

Erasmus Scholarship, 2013, 2015

WORK EXPERIENCE

University of California, San Francisco, Department of Surgery 06/2016 – 11/2017
Visiting Scholar *San Francisco, USA*

· Translation of novel medical technologies into transformative new devices and treatments to improve human health.

Vienna University of Technology, Faculty of Chemistry 09/2016 – 06/2017
Project assistant *Vienna, AT*

· Cell Chip Group: Development of implantable biosensors for tissue rejection monitoring

AIT - Austrian Institute of Technology, Biosensor Technologies 09/2015 – 06/2016
Working student *Vienna, AT*

· Cell Chip Group: Biosensor technologies and Microfluidics

Siemens AG Corporate Technology, Innovative Ventures 02/2015 – 06/2015
Working student *München, DE*

· Validation and optimisation of immunomagnetic cell labeling method (CD4+) by using fluorescence-activated cell sorting and magnetic flow cytometry

Siemens AG Corporate Technology, Research and Technology Center 07/2013 – 10/2013
Intern *Erlangen, DE*

· Time-of-flight magnetic flow cytometry in whole blood
· Experimental work on rapid prototype microfluidic chips in the clean room

Science Center Network 03/2013 – 07/2015
Explainer *Vienna, AT*

· Communicating science and research and run museum operations and scientific workshops for children

Styria Media Group AG 09/2011 – 10/2015
Economic Journalist/Freelancer *Vienna, AT*

· Investigative research for the magazine "Business People"

Danube Hospital 07/2005 – 06/2010
Chef de Partie, Dietary Chef *AT, HU*

· Pre-academic work as a chef, diatery expert and kitchen manager in various restaurants and hospital dietary departments

EXTRACURRICULAR ACTIVITIES

National Board of Austrian Student's Union 06/2015 – 03/2016
International Officer *Vienna, AT*

· Representative at ESU - European Students Union

University of Natural Resources and Applied Sciences, Vienna 10/2013 – 02/2017
International Officer & Student Representative *Vienna, AT*

· Head of Department of International Affairs at Student's Union
· Task Force member of ELLS - Euroleague for Life Sciences
· Main member at Studies Committee of Food Sciences and Biotechnology

LANGUAGE SKILLS

Hungarian	native speaker
German	fluent (spoken and written)
English	professional (spoken and written)

IT SKILLS

Operating Systems	Advanced knowledge of Mac OSX and Microsoft environments
Software	MS-Office package, Latex, OpenOffice, OriginLab, CS5, InDesign
CMS	Basic programming knowledge

REFERENCES

Available on request.